

HYSTERETIC MODELS FOR REINFORCED CONCRETE SHEAR WALLS IN
NUCLEAR FACILITIES USING NSGA-II AND DATA-DRIVEN TECHNIQUES

**HYSTERETIC MODELS FOR REINFORCED CONCRETE SHEAR WALLS IN
NUCLEAR FACILITIES USING NSGA-II AND DATA-DRIVEN TECHNIQUES**

By

Samarapreet Singh

B.Eng., E.I.T

A Thesis submitted to the Civil Engineering School of Graduate Studies in Partial Fulfillment of
the Requirements for the Degree of
Master of Applied Science
McMaster University

© Samarapreet Singh, April 2024

MASTER OF APPLIED SCIENCE (2024)

McMaster University

CIVIL ENGINEERING

Hamilton, Ontario

Title: Hysteretic Models for Reinforced Concrete Shear Walls in Nuclear Facilities Using NSGA-II and Data-Driven Techniques

Author: Samarapreet Singh, B.Eng. (McMaster University)

Supervisor: Dr. Mohamed Ezzeldin

Number of pages: viii, 69

Abstract

The current thesis provides a thorough exploration of the seismic behaviour of reinforced concrete (RC) shear walls, with a particular focus on the performance characteristics of squat RC shear walls, which are pivotal for the seismic resilience of safety-related structures in nuclear facilities. The thesis is rooted in the application of the Bouc-Wen-Baber-Noori (BWBN) model, an advanced hysteretic model that captures the complex nonlinear response of materials under cyclic loading. The primary objective is to simplify the predictive aspect of the hysteretic response of squat RC shear walls through a multifaceted framework that integrates the BWBN model with data-driven techniques. Specifically, the thesis adopts the non-dominated sorting genetic algorithm (NSGA-II) for the optimization of the BWBN model parameters through a dataset of 100 squat RC shear wall specimens that were collected from previous relevant experimental programs. The thesis then utilizes the BWBN model results through genetic programming to develop equations for the different model parameters. The developed framework is expected to provide a practical tool for engineers and practitioners, simplifying the incorporation of complex hysteretic behaviours in the seismic design and assessment of squat RC shear walls. The extended analysis and findings presented in the current thesis underscore the critical importance of adopting sophisticated computational techniques in the field of earthquake engineering. By advancing our understanding of the seismic behaviour of RC shear walls and improving the tools available for their analysis, this research contributes significantly to the ongoing efforts to enhance the resilience of nuclear facilities in the face of extreme seismic events.

Keywords: Bouc-Wen-Baber-Noori Model; Genetic Programming; Hysteretic Model; NSGA-II Optimization; Reinforced Concrete Shear Walls.

Acknowledgements

As I pen down this acknowledgment, my heart is brimming with gratitude towards those who have been my pillars of support throughout this enlightening journey. Foremost, I extend my deepest appreciation to my parents, whose unwavering faith and boundless love have been my constant source of strength. To my mother, in particular, I owe an immeasurable debt of gratitude. Her sacrifices, encouragement, and unconditional love have sculpted me into the individual I am today. Her belief in my potential has been the guiding light through my darkest hours, propelling me towards achieving this milestone. I am equally grateful to my sister, whose belief in me never faltered. Her confidence in my abilities has been a source of comfort and motivation, encouraging me to strive for excellence in every endeavour. Her role in my life has been paramount, and for that, I am forever thankful. To my cousins, who have been my comrades in this voyage, I extend my heartfelt thanks. Your assistance, camaraderie, and the countless ways you've supported me have enriched my journey immeasurably. The collective memories of our shared experiences will always hold a special place in my heart.

Most importantly, I wish to express my profound gratitude to my supervisor, Dr. Mohamed Ezzeldin. His guidance, patience, and unwavering support have been the cornerstone of my academic journey. Dr. Ezzeldin's belief in my capabilities, even when I doubted myself, has been a source of inspiration and courage. His mentorship extended beyond academic guidance; it was his empathetic approach during challenging times that made all the difference. For always being in my corner and helping me navigate through the tough times, I am eternally grateful.

To all of you who have been a part of this journey, I extend my sincerest thanks. This achievement is not solely mine but a testament to the collective support, faith, and love that each one of you has bestowed upon me. Thank you for being my guiding stars.

Table of Contents

1. Introduction.....	1
1.1 Research Significance	5
2. Background of Hysteretic Models	7
2.1 Bouc-Wen (BW) Model	8
2.2 Bouc-Wen-Baber-Noori (BWBN) Model.....	10
3. Non-dominated Sorting Genetic Algorithm (NSGA-II)	13
4. Methodology.....	15
5. Squat RC Shear Wall Dataset.....	17
5.1 Wall Parameter Description	17
6. NSGA-II Toolbox Architecture	21
6.1 Background of NSGA-II	21
6.2 BWBN Parameters Using NSGA-II.....	23
6.3 Hysteretic Behaviour Validation	31
7. Data Management.....	35
7.1 Exploratory Data Analysis.....	Error! Bookmark not defined.
7.1.1 Data Cleaning and Transformation	35
7.1.2 Visualization of Data.....	35
7.1.3 Correlation Analysis.....	38
8. Genetic Programming.....	44
8.1 Genetic Programming Procedure.....	46
8.2 Genetic Programming Utilization and Results	50
9. Conclusion.....	57
10. References	59

List of Figures

Figure 1: Methodology Flowchart for Developing the BWBN Model Parameters of Squat RC Shear Walls	17
Figure 2: The Number of Squat RC Shear Walls Corresponding to their Different Geometrical Characteristics and Design Parameters	21
Figure 3: Experimental versus NSGA-II Results for Different Squat RC Shear Walls	34
Figure 4: Scatterplots of Squat RC Shear Walls Corresponding to Different Parameters.....	38
Figure 5: Correlation Matrices for the Different Wall and BWBN Parameters	42
Figure 6: A Correlation Matrix for the Different BWBN Parameters	43
Figure 7: Evolutions of GP Individuals (Expressions) throughout Generations	47
Figure 8: Example of GP Individual Represented as a Mathematical Expression and a Corresponding Tree-Shaped Structure.....	48
Figure 9: Flowchart Representation of GP Procedure Based on the Study by Koza (1992)	49

List of Tables

Table 1. Summary of the Bouc-Wen (BW) And Bouc-Wen-Baber-Noori (BWBN) Parameters and their Corresponding Purposes within the Hysteretic Responses.....	13
Table 2. Geometrical Characteristics and Design Parameters for the Collected Squat RC Shear Walls	17
Table 3. The BWBN Parameters Used in the NSGA-II Toolbox.....	24
Table 4. The BWBN Parameter Values for the 100 Squat RC Shear Walls Based on the NSGA-II Toolbox.....	24
Table 5. The BWBN Parameter Values for the 100 Squat RC Shear Walls Based on the NSGA-II Toolbox.....	28

List of Acronyms

BW: Bouc-Wen Model
 BWBN: Bouc-Wen-Baber-Noori Model
 NSGA-II: Non-dominated Sorting Genetic Algorithm II
 SDOF: Single Degree of Freedom
 GP: Genetic Programming
 RC: Reinforced Concrete
 MSE: Mean Squared Error

List of Equations

Equation 1	8
Equation 2	8
Equation 3	8
Equation 4	10
Equation 5	10
Equation 6	10
Equation 7	10
Equation 8	11
Equation 9	11
Equation 10	11
Equation 11	11
Equation 12	11
Equation 13	12
Equation 14	14
Equation 15	22
Equation 16	22
Equation 17	22
Equation 18	23
Equation 19	53
Equation 20	53
Equation 21	53
Equation 22	54
Equation 23	54
Equation 24	54
Equation 25	54
Equation 26	55
Equation 27	55
Equation 28	55
Equation 29	55
Equation 30	55
Equation 31	56
Equation 32	56
Equation 33	56
Equation 34	56

1. Introduction

Reinforced concrete (RC) shear walls are one of the most common structural elements used in the modern construction industry. The intrinsic properties of such walls offer an optimal blend of strength, rigidity, and flexibility—crucial for modern architectural demands. Therefore, such walls are frequently used in multi-storey structures to carry gravity loads from the flooring system (e.g., dead and live loads) and resist lateral loads such as seismic and wind loads. For the latter loads, RC shear walls are an immensely proper choice when it comes to seismic force-resisting systems (SFRS) for high-rise buildings. Such walls have been extensively used all over the world, especially in Canada, as their strategic employment within these buildings allows architects and engineers to explore innovative design alternatives without compromising the safety of such buildings. This extensive use is mainly attributed to that the dynamic performance of these shear walls under lateral loads ensures that their buildings remain resilient, even in seismic-prone areas (NBCC 2020; CSA 23.3)

There are many distinct types of RC shear walls including ductile shear walls, moderate ductile shear walls and squat shear walls. The attributes of ductile and moderate ductile shear walls are obvious from their names as these wall systems are typically designed to experience flexure failures, thus protecting their structures when subjected to extreme seismic events. Specifically, the National Building Code of Canada (NBCC 2020) and relevant design standards (e.g., CSA A23.3) specify that such wall systems should be designed based on the capacity design principle, which means that flexure failures of these walls are considered the safety “fuse” (plastic hinge) of their structures.

Squat RC shear walls are commonly used as the main SFRS of safety-related structures in nuclear facilities. Within these critical built infrastructure systems, such walls are much longer

(i.e., 6-90 m) and thicker (i.e., 0.5-2 m) with no openings to prevent any possibilities of radiation leakage while enhancing blast/fire protection levels (Abouyoussef and Ezzeldin 2023), thus resulting in walls with height-to-length ratios less than 2 (i.e., squat walls). These geometrical constraints (i.e., low aspect ratios) lead to unique challenges because such squat RC shear walls, unlike ductile and moderate ductile RC shear walls, typically experience brittle shear failures with limited displacement ductility demands after yielding. Specifically, squat RC shear walls experience mainly shear and sliding failures, thus rapidly losing their strength and stiffness even with small increments of inelastic deformations. Although it remains challenging to accurately predict such brittle failures during earthquake events, it is crucial to quantify the dynamic performance of squat shear walls and establish relationships amongst their geometrical configurations and design parameters. This is essential to ensure the resilience of such walls under extreme seismic events, not only from an engineering standpoint but also from the perspective of public safety and environmental protection given their wide applications in critical built infrastructure systems such as nuclear reactor structures.

The overall behaviour of structural systems under lateral loads can be quantified through hysteretic models. Such models can portray a very deep perception of how structural systems behave under different seismic demands, and therefore, such models are considered a very effective and crucial tool in earthquake engineering. In this respect, the seismic performance of several RC systems (e.g., wall deformations, pinching characteristics, and energy dissipation capacities) was quantified in previous research studies by a wide range of macroscale hysteretic models that encompass single/multiple component models, truss models, and multi-spring models.

In general, macroscale hysteretic models can mostly be categorized into piecewise linear or polygonal hysteretic models and smooth hysteretic models. In piecewise linear or polygonal

hysteretic models, such as the bilinear degrading stiffness model (Clough and Johnston 1966), trilinear Takeda model (Takeda et al. 1970), bilinear SINA hysteresis model (Saidi and Sozen 1979), deviations in stiffness occur at discrete stages such as the elastic, cracking, yielding, strength and stiffness degradation, crack, and gap closing stages. Conversely, in smooth hysteretic models, such as the Bouc-Wen-Baber-Noori model (Baber and Noori 1985), continuous changes in stiffness occur due to yielding; however, sharp changes occur due to unloading and deteriorating behaviour (Baber and Wen 1981).

The aforementioned hysteretic models were utilized in previous studies to quantify the seismic performance of RC structures. For example, Kabeyasawa et al. (1983) developed a three-vertical-line elements model (TVLEM) using infinite rigid beams at the bottom and top floor levels to replicate a pseudo-dynamic earthquake response of a full-scale seven-story RC wall frame structure. In this model, two truss elements were used to symbolize the axial stiffness of the boundary elements, in which the central one-component vertical element containing a vertical spring, a horizontal spring, and a rotational spring, denoted the wall panel. In addition, Vulcano and Bereto (1987) altered the outer vertical spring of the TVLEM model by using i) a spring assembly that comprised a single topmost spring to denote the uncracked concrete; and ii) two parallel springs to represent the cracked concrete and steel. Vulcano et al. (1988) substituted the rotational spring with additional vertical springs to simulate the axial behaviour and the yielding of the vertical reinforcement within the concrete. Sittipunt and Wood (1993) also introduced microscale finite element methods to investigate the cyclic behaviour of RC slender walls. Moreover, Linde and Bachmann (1994) developed a microelement to represent the inelastic seismic behaviour of shear walls controlled by flexure, with a modest influence of shear cracking in the cyclic response. In addition, Youssef and Ghobarah (1999) established a macro wall element

consisting of four steel and concrete springs to represent the behaviour of steel reinforcement and concrete strut within the plastic hinge region, while a pair of diagonal springs was used to characterize the shear behaviour of the wall. The analytical model by Hidalgo et al. (2002) was also able to predict the inelastic seismic response of reinforced concrete shear-wall buildings, including both shear and flexure failures. Greifenhagen (2005) developed an analytical model with a plastic hinge over the entire height of the squat shear wall to derive a rationale for its shear strength envelope when subjected to cyclic loading. The multilayer model by Belmouden and Lestuzzi (2007), created from an inelastic beam element and interface bond-slip sub-elements, captured the seismic hysteretic behaviour of RC structural walls. Gulec (2009) opted for finite element methods and modelled RC walls with and without boundary elements using Vector2 and ABAQUS. Soltani et al. (2011) also adopted a fibre section model using *OpenSEES* (McKenna et al. 2008) to simulate the cyclic behaviour of RC walls.

Plastic hinge areas that are developed within RC structural elements result in non-linear behaviour under severe ground excitations. Under these circumstances, such elements typically show significant non-linear hysteresis due to unpredictable restoring forces. To understand and analyze the seismic response of these RC structural elements, it is crucial to develop ways to model this highly non-linear behaviour so that adequate design procedures can be followed, especially in plastic hinge areas. For these reasons, some researchers (e.g., Ikhoulane and Rodellar, 2007; Sues, Mau, and Wen, 1988; Oussar and Dreyfus, 2001) have developed alternative models called “semi-physical” models, where these models combine some physical understanding with advanced mathematical models.

Squat RC shear walls encounter hysteretic non-linear behaviour in which the dynamic relation amongst their variables is memory-based (Ikhoulane, Mañosa, and Rodellar, 2003).

Specifically, the complex nature of squat RC shear walls during and after an earthquake includes non-linear restoring forces that are difficult to portray as a single function of the instantaneous displacement and velocity. Therefore, several hysteretic models were developed overtime to capture these time-dependent attributes using complex sets of differential equations (e.g., Charalampakis and Dimou, 2010; Masaru and Aiken, 1997; Sireteanu, Mitu, Giuclea, and Solomon, 2014). However, among such hysteretic models, the Bouc-Wen-Baber-Noori (BWBN) model was demonstrated to achieve acceptable hysteretic response for RC structures.

1.1 Research Significance

The BWBN model is extremely complex because the model involves numerous unknown variables that need to be identified, with a substantial numerical convolution. As such, from a practical engineering point of view, implementing the BWBN model in the design procedures is a challenging task because there is a scarcity of comprehensive studies that offer ready-to-use equations that are tailored for predicting the hysteretic response of squat RC shear walls. Further complicating matters, the available literature on RC shear walls often considers a simplified approach by optimizing just one parameter (e.g., errors in energy dissipation capacities), potentially leading to imprecise representations and conclusions for all remaining wall parameters (e.g., errors in displacement capacities).

In response to these glaring gaps, the current thesis embarks on a multifaceted framework. The *first* objective of this framework is to meticulously implement the BWBN model for a single-degree-of-freedom (SDOF) system, aiming to intricately develop degradation and pinching characteristics pertinent to squat RC shear walls. As such, it was crucial to gather a vast database, consisting of 100 squat RC shear wall specimens, contributed by a myriad of esteemed researchers spanning the globe. Utilizing these wall specimens from previous studies not only offers a rich and

diverse dataset but also paves the way for judicious use of resources, underscoring the robustness and efficiency of the adopted framework.

Standing at the brink of an era characterized by unmatched computational capabilities, it is essential for the research community to seamlessly integrate current datasets with the latest analytical methodologies. Consistent with this principle, the *second* objective of the developed framework focuses on leveraging the non-dominated sorting genetic algorithm II (NSGA-II), a pioneering multi-objective genetic algorithm (MOGA) approach, to estimate the BWBN hysteretic parameters in an effort to accurately simulate the cyclic response of squat RC shear walls. Unlike many of its predecessors, the framework adopted here emphasizes the optimization of multiple wall parameters, paving the way for a more holistic understanding. This objective also facilitates identifying potential correlations among various BWBN hysteretic parameters. Specifically, through this objective, relevant researchers can provide more precise insights into the behaviour of squat RC shear walls. Enhancing this effort, researchers can also utilize an array of contemporary data analysis tools, encompassing both sophisticated supervised and unsupervised machine learning methodologies, all aimed at discovering intricate correlations and subtleties among wall parameters.

Diving deeper into the analytical realm, the *third* objective of this framework emerges with a keen focus on practical applications. Amidst the vast sea of data and parameters derived from sophisticated algorithms, there exists an immediate need for practitioners to have simplified, yet highly effective, tools at their disposal. To cater to this need, the current thesis adopts genetic programming as a cornerstone for the creation of ready-to-use equations. These equations, meticulously tailored for the BWBN hysteretic parameters of squat RC shear walls, are aimed at streamlining the process of understanding and applying the insights gleaned from the NSGA-II

analysis. By taking this path, the objective resonates with the pressing demand for the immediate applicability of research outcomes. More than just an academic exploration, this objective underscores the translation of complex datasets and multi-objective outcomes into actionable, user-friendly, and efficient solutions that both researchers and practicing engineers can readily integrate into their repertoire. In essence, by fusing the computational prowess of genetic programming with the foundational principles of structural engineering, we strive to bridge the gap between theoretical advancements and practical applications, ensuring the seamless dissemination of knowledge across the community.

2. Background of Hysteretic Models

One of the most effective models that were used to simulate the hysteretic behaviour of systems through differential equations is the Bouc-Wen (BW) model (Bouc, 1971; Wen, 1976). This model has been utilized in numerous applications throughout the various engineering disciplines. Some of the applications include simulating highly asymmetric hysteretic systems (Song and Kiureghian, 2006), predicting the seismic response of unbonded fibre-reinforced elastomeric isolators (Manzoori and Toopchi-Nezhad, 2017), evaluating the damage of hysteretic degrading structures including mechanical degradation (Marano and Greco, 2006), investigating the cyclic response of steel cantilever beams (Charalampakis and Koulouris, 2008), and simulating strain hardening effects during earthquake excitations (Kottari, Charalampakis, and Koumoussis, 2014). These include many other applications that were explored by various researchers (e.g., Sireteanu, Giuclea, and Mitu, 2010; Betti, Facchini, and Vignoli, 2015; Charalampakis, 2015; Zhu and Rui, 2016; Solovyov, Semenov, Meleshenko, and Barsukov, 2017).

2.1 Bouc-Wen (BW) Model

In the current subsection, the BW model is introduced using the equation of motion and the corresponding variables. The equation of motion for an SDOF system that is subjected to an external excitation can be stated as:

$$m\ddot{x} + c\dot{x} + F_T[x(t), z(t), t] = F(t), \quad \text{Equation 1}$$

where m is the mass of the system; x is the relative displacement of the system with respect to the ground motion; c is the linear viscous damping coefficient; $F_T[x(t), z(t), t]$ is the non-damping restoring force; and $F(t)$ is the time-dependent external excitation. The “dot” accents on top of x parameters represent the derivatives of displacement with respect to time. Therefore, \dot{x} and \ddot{x} represent the velocity and acceleration, respectively (Pellicciari et al. 2018).

According to the BW model, the restoring force is presented by the following expression:

$$F_T[x(t), z(t), t] = \alpha k_i x(t) + (1 - \alpha) k_i z(t), \quad \text{Equation 2}$$

Where $\alpha k_i x(t)$ represents the linear or the elastic component of the system, while $(1 - \alpha) k_i z(t)$ is the hysteretic component, which is contingent on the history of stresses and strains that the system experiences throughout its lifespan. Additionally, k_i is the elastic stiffness of the system and α is the stiffness ratio (i.e., defined as the ratio of final asymptote tangent stiffness, k_f , to the initial stiffness, k_i , hence $0 \leq \alpha \leq 1$). Also, $z(t)$ is the hysteretic displacement that is defined as a fictitious displacement that governs the hysteretic restoring force, which is given by the following differential equation:

$$\dot{z}(t) = A\dot{x}(t) - (\beta|\dot{x}(t)||z(t)|^{n-1}z(t) + \gamma\dot{x}(t)|z(t)|^n), \quad \text{Equation 3}$$

with the initial condition $z(0) = 0$. The parameters β , γ and n control the shape of the hysteretic cycle, while A determines the tangent stiffness.

The BW model has notable limitations in capturing effectively specific behaviours such as strength degradation, stiffness degradation, and pinching effects, especially in RC shear walls (Ismail, Ikhouane, and Rodellar, 2009). In an attempt to overcome these limitations, Baber and Noori (1985) introduced an enhanced version, termed the Bouc-Wen-Baber-Noori (BWBN) model. This model, while adept at reflecting the pinching and degradation effects, is intricate. Specifically, the model contains a range of complex functions and a multitude of unknown parameters awaiting identification, which inevitably leads to a convoluted numerical landscape. From an applied engineering perspective, the BWBN model, with its inherent complexities, poses challenges to be operationalized by researchers and practicing engineers (Baber and Noori, 1985; Ortiz, Alvarez, and Bedoya-Ruíz, 2013; Peng, Li, Du, Deng, and Alici, 2014). Infusing such a detailed model into conventional design methodologies becomes cumbersome, given the significant computational exertion it demands and the increased possibility of errors during the intricate identification processes. Especially in scenarios necessitating quick decisions or real-time analyses, relying on the BWBN model may not be pragmatic due to several challenges associated with its extensive computational demands.

Many researchers acknowledged these challenges and subsequently ventured into devising modified versions of the BW model. The primary objective was to retain the capability of representing pinching and degradation effects while stripping away the complexities associated with the BWBN model. A modified BW model was devised by Pellicciari et al. (2018) which aimed at striking a balance between accuracy and simplicity. This modified BW model relied on introducing a physics-based formulation, reducing the number of parameters, and simplifying the identification process, thus making it a more viable option for engineering applications, where a combination of accuracy and simplicity is often desired. However, introducing fewer parameters

for the modified BW model also reduced the accuracy and precision of the results in contrast to the results produced by the BWBN model for the same specimens (Pellicciari et al., 2018).

2.2 Bouc-Wen-Baber-Noori (BWBN) Model

In the BWBN model, the equation of motion of the SDOF system (i.e., Equation 1) and the restoring force equation (i.e., Equation 2) remain the same. However, the inherent law that illustrates the hysteretic displacement $z(t)$ is extended, as presented in the following equation:

$$\dot{z}(t) = h(z(t)) \times \left[\frac{A(\epsilon)\dot{x}(t) - \nu(\epsilon)(\beta|\dot{x}(t)||z(t)|^{n-1}z(t) + \gamma\dot{x}(t)|z(t)|^n)}{\eta(\epsilon)} \right],$$

Equation 4

with the initial condition $z(0) = 0$. Equations 3 and 4 are similar in some ways, where the $\beta|\dot{x}(t)||z(t)|^{n-1}z(t) + \gamma\dot{x}(t)|z(t)|^n$ term is similar in both equations. The additional parameters $\nu(\epsilon)$ and $\eta(\epsilon)$ are degradation functions that take into consideration the strength and stiffness degradation effects, respectively. $A(\epsilon)$, $\nu(\epsilon)$ and $\eta(\epsilon)$ are defined as linearly increasing functions of $\epsilon(t)$ as:

$$A(\epsilon) = A_0 - \delta_A \epsilon(t),$$

Equation 5

$$\nu(\epsilon) = \nu_0 - \delta_\nu \epsilon(t),$$

Equation 6

$$\eta(\epsilon) = \eta_0 - \delta_\eta \epsilon(t),$$

Equation 7

where the δ_A , δ_ν and δ_η parameters determine the rate of stiffness and strength degradation. Hence, a value of zero assigned to such variables ($\delta_A = \delta_\nu = \delta_\eta = 0$) would mean that the element has no degradation. Conversely, when these parameters have non-zero values ($\delta_A, \delta_\nu, \delta_\eta \neq 0$), the element has some type of degradation narrative. Since the parameter $A(\epsilon)$ is somewhat redundant as both

the hysteretic stiffness and hysteretic force can be varied by the stiffness ratio and the hysteretic shape parameters, it can have a unit value (i.e., $A(\epsilon) = 1$), as verified by Sengupta and Li (2014).

The time-dependent function for the absorbed hysteretic energy $\epsilon(t)$ represents the energy dissipated by the system and it is defined as the area under the mass normalized hysteretic restoring force $F^h(z(t)) = (1 - \alpha)k_i z(t)$ versus the total displacement. Therefore, the total dissipated hysteretic energy per unit mass can be quantified as:

$$\epsilon(t) = \int_{x(0)}^{x(t)} \frac{F^h(x)}{m} dx = (1 - \alpha)\omega_0^2 \int_0^t z(\tau)x(\tau)d\tau,$$

Equation 8

Additionally, the term $h(z(t))$ in Equation (4) represents the pinching function and it is expressed as:

$$h(z(t)) = 1 - \varsigma_1(\epsilon) e^{\left(\frac{-|z(t)\text{sign}(\dot{x}(t)) - qz_u|^2}{\varsigma_2(\epsilon)^2} \right)},$$

Equation 9

where $\text{sign}(\dot{x}(t))$ is the signum function of $x(t)$, q is a constant value and z_u is the ultimate value of $z(t)$, defined as:

$$z_u = \sqrt[n]{\frac{1}{v(\epsilon)(\beta + \gamma)'}}$$

Equation 10

The parameter $\varsigma_1(\epsilon)$ varies from 0 to 1; where both $\varsigma_1(\epsilon)$ and $\varsigma_2(\epsilon)$ vary with the hysteretic energy as expressed by the following equations:

$$\varsigma_1(\epsilon) = \varsigma_0(1 - e^{-p\epsilon(t)}),$$

Equation 11

$$\varsigma_2(\epsilon) = (\psi + \delta_\psi \epsilon(t))(\lambda + \varsigma_1(\epsilon)),$$

Equation 12

where ζ_0 measures the total slip; p represents a constant that is responsible for controlling the rate of the initial drop in the slope; ψ is a factor that contributes to the pinching behaviour; δ_ψ is a specified constant parameter that measures the dispersion rate of the pinching phenomenon; and λ is a parameter that controls the variation of the parameters $\zeta_1(\epsilon)$ and $\zeta_2(\epsilon)$ (Sengupta and Li, 2013). Therefore, the parameters mentioned above ζ_0 , p , ψ , δ_ψ , λ and q express the form of the pinching phenomenon. When $h(t) = 1$, this indicates that pinching is not considered in the model.

Furthermore, in the original BWBN model, the stiffness ratio α was deemed to be of constant value throughout. However, based on experimental results of RC shear walls under cyclic loading, it was observed that the stiffness was reduced well after attaining a certain displacement (Sengupta and Li, 2014). Therefore, considering the stiffness ratio of constant magnitude is somewhat impractical, hence stiffness ratio α can be represented as a function of D_{max} :

$$\alpha = \alpha_0 e^{(-0.1D_{max})}$$

Equation 13

where α_0 is the value of the stiffness ratio when the displacement is zero and D_{max} is the maximum positive and the absolute maximum negative displacement for $u > 0$ and $u < 0$, respectively. However, to reduce the complexity of an inherently complex model, the original BWBN model's assumptions were kept intact without any modifications.

To clearly explain the roles of each parameter in defining the shape and progression of the hysteretic cycles of the model, Table 1 summarizes the entire set of parameters for both the BW and BWBN models (Pellicciari et al., 2018; Ajavakom, Ng, and Ma, 2008). As can be seen in the table, the BWBN model can represent the hysteretic response of RC shear walls with several

parameters that enhance its accuracy when compared to those of the BW model; however, the former model tremendously increases the computational complexity.

Table 1. Summary of the Bouc-Wen (BW) And Bouc-Wen-Baber-Noori (BWBN) Parameters and their Corresponding Purposes within the Hysteretic Responses

	Parameter	BW	BWBN	Purpose
1	α	Yes	Yes	Ratio of linear to nonlinear response
2	A	Yes	Yes	Basic hysteresis shape control
3	β	Yes	Yes	Basic hysteresis shape control
4	γ	Yes	Yes	Basic hysteresis shape control
5	n	Yes	Yes	Sharpness of yield
6	ν_0		Yes	Strength degradation
7	δ_ν		Yes	Strength degradation
8	η_0		Yes	Stiffness degradation
9	δ_η		Yes	Stiffness degradation
10	p		Yes	Pinching slope
11	q		Yes	Pinching initiation
12	ζ_0		Yes	Measure of total slip
13	ψ		Yes	Pinching magnitude
14	δ_ψ		Yes	Pinching rate
15	λ		Yes	Pinching severity

3. Non-dominated Sorting Genetic Algorithm (NSGA-II)

Most of the available studies related to the Bouc-Wen model or its extended versions such as the BWBN models have predominantly used single-objective functions through evolutionary algorithms to calibrate their underlying models. This single-objective approach typically employs a mean square error (MSE) that captures the deviation between the known displacements and the estimated ones (Sengupta and Li, 2014). While this approach has shown success in many applications, it tends to focus solely on minimizing a specific parameter, potentially overlooking other critical parameters of the system's behaviour.

In contrast, utilizing multi-objective optimization algorithms, such as the Multi-Objective Genetic Algorithm (MOGA), allows for a more comprehensive understanding of the behaviour of

the underlying structural elements. The MOGA simultaneously optimizes multiple objectives, providing a set of optimal solutions (known as Pareto solutions) that showcase the trade-offs among these objectives (Ortiz, Alvarez, and Bedoya-Ruíz, 2013). By considering multiple objectives, the approach can, for instance, balance between minimizing displacement errors and preserving other crucial performance parameters, such as energy dissipation and stiffness degradation, which may be overlooked in single-objective optimization functions. This comprehensive view provided by the MOGAs can lead to a more realistic and holistic understanding of the behaviour of the structural elements. For RC shear walls, all previous studies have traditionally adopted single-objective functions. In addition, because squat RC shear walls are complex entities with multiple interacting parameters, a multi-objective function could provide richer insights into their behaviour, especially when multiple performance measures are of interest.

The non-dominated sorting genetic algorithm (NSGA-II) is used in the current thesis given its good performance in obtaining multiple solutions in uni-modal and multi-modal continuous and discontinuous functions. Specifically, the NSGA-II is used herein to identify the BWBN model parameters that are presented earlier in Table 1. The NSGA-II has four objectives when used herein to optimize for the best solution: i) the weighted error between displacements; ii) the maximum error between displacements; iii) the difference between the total dissipated energy per unit mass; and iv) the maximum error between the dissipated energy per unit mass. The general multi-objective optimization problem is expressed as below:

$$\begin{aligned} & \text{Minimize: } f(p) \\ & \text{subject to: } g(p) \geq 0 \text{ \& } h(p) = 0, \end{aligned}$$

Equation 14

where the $f(p) \in R^m$ are the objective functions; $p \in D \subseteq R^q$ is the vector of parameters; $g(p)$ is the set of inequality constraints; $h(p)$ is the set of equality constraints; and D is the parameter space.

The notion here is to achieve an appropriate choice of parameters that represent and predict the hysteretic behaviour of structural elements. The tuned parameters are represented by vector p . In the current work, squat RC shear walls are obtained from literature and then processed through the NSGA-II to obtain the BWBN model parameters that express the hysteretic relationship of such walls. The four objective functions are minimized to identify the parameters p , as discussed in a later section.

4. Methodology

In the pursuit of understanding the complex hysteretic behaviour of squat RC shear walls, the current thesis develops a multifaceted framework that is divided into systematic sequential steps, as presented in Figure 1. The foundational step encompasses a rigorous literature review that aims at collecting existing research articles, experimental results, and reports that mainly focus on the hysteretic behaviour of squat RC shear walls. Through a blend of both primary and secondary data, an expansive dataset of squat RC shear walls and their corresponding design parameters is created, which serves as the cornerstone for the successive endeavours of the work presented herein.

Following the collection of this dataset, the NSGA-II is employed as a primary computational tool. As discussed earlier, the strength of the NSGA-II resides in its ability to efficiently handle multi-objective optimization. As such, the goal of this step is to utilize the NSGA-II along with the collected dataset in order to identify and experimentally validate the

BWBN model parameters for each wall in a manner that addresses multiple conflicting objectives simultaneously.

While data acquisition is crucial, understanding this data is equally paramount. Therefore, the following step within the developed methodology is to present a preliminary description of the BWBN model parameters and their potential relations with the different wall geometrical configurations and design parameters. Specifically, exploratory data analysis is performed to uncover the inherent relationships within the data by listing all the parameters and subsequently narrowing them down through rigorous selection procedures in an effort to focus on the key variables.

Following the preliminary data analysis, the use of genetic programming is an integral step of the methodology to: 1) further refine the identification process and validate the findings of the former step; and 2) develop ready-to-use equations for all the BWBN model parameters in terms of the wall geometrical parameters and design parameters. In this step, the dataset is divided into development and validation subsets to introduce equations that can achieve the balance between accuracy and generalizability in terms of predicting the hysteretic behaviour of squat RC shear walls.

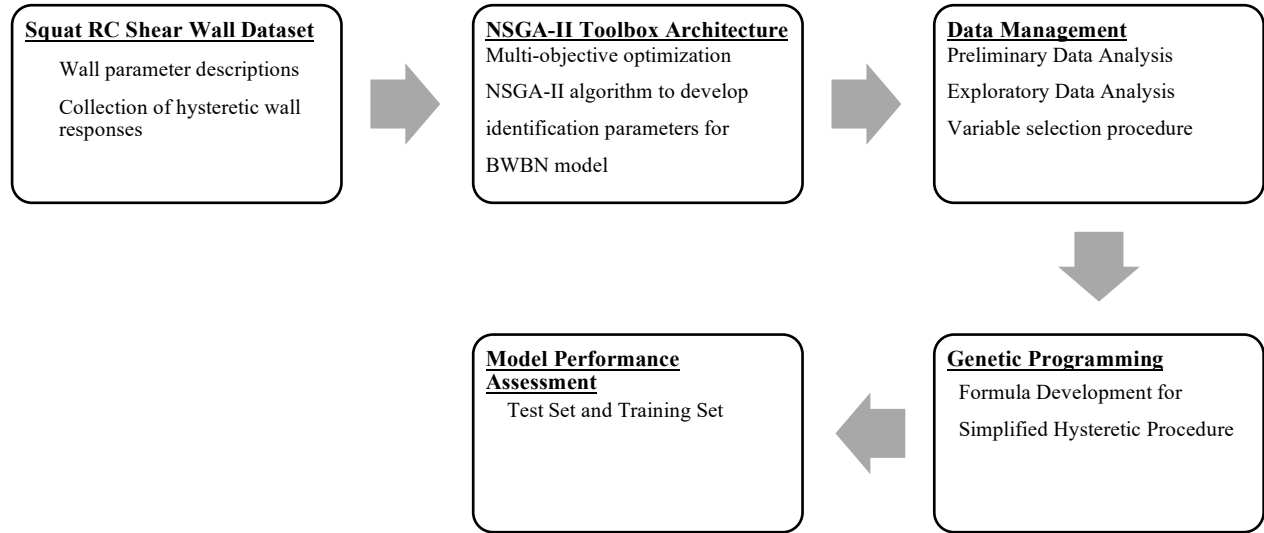


Figure 1: A Multifaceted Framework for Developing the BWBN Model Parameters of Squat RC Shear Walls

5. Squat RC Shear Wall Dataset

5.1 Wall Parameter Description

The objective of the current thesis is to predict the BWBN parameters for squat RC shear walls in order to quantify their hysteretic responses. However, to predict such parameters using data-driven techniques such as regression, clustering, or genetic programming, it is key to understand the underlying dataset. Nine wall geometrical characteristics and design parameters are selected herein to represent the identity of each squat RC shear wall, as presented in Table 2.

Table 2. Geometrical Characteristics and Design Parameters for the Collected Squat RC Shear Walls

Wall ID	l_w (mm)	h_w (mm)	t_w (mm)	f'_c (Mpa)	f_y (Mpa)	ρ_h (%)	ρ_v (%)	ρ_{be} (%)	n (%)
Beko 1	3000	1200	400	54	500	0.71	0.47	1.7	0
Beko 4	3000	1200	400	54	500	0.71	0.47	1.7	0
ChengH115	2032	1905	203.2	44	785	0.4	0.312	9.7	0
ChengH60	2032	1905	203.2	44	413	0.8	0.562	9.7	0
ChengH60X	2032	1905	203.2	42	413	0.8	0.562	9.7	0
ChengM115	2032	1905	203.2	38	785	0.147	0.103	9.7	0
ChengM60	2032	1905	203.2	39	413	0.293	0.21	9.7	0

Greifenhagen M1	1000	610	100	50.69	504	0.37	0.3	0	1
Greifenhagen M2	1000	610	100	50.98	504	0	0.3	0	2.2
Greifenhagen M3	900	610	80	20.1	504	0.3	0.3	0	4.4
Greifenhagen M4	900	610	80	24.4	624	0.26	0.3	0	5
Hirosawa 72	1700	1600	160	17.3	410	0.26	0.51	5.68	11.4
Hirosawa 73	1700	1600	160	20.8	410	0.26	0.51	5.68	9.4
Hirosawa 74	1700	1600	160	20.8	410	0.57	0.51	5.68	9.4
Hirosawa 75	1700	1600	160	13.7	410	0.57	0.51	5.68	14.3
Hirosawa 76	1700	1600	160	14.7	410	1.08	0.51	5.68	13.3
Hirosawa 77	1700	1600	160	18.3	410	1.08	0.51	5.68	10.7
Hirosawa 80	1700	1600	160	14.7	410	1.08	0.51	2.51	13.3
Hirosawa 81	1700	1600	160	18.3	410	1.08	0.51	2.51	10.7
Hirosawa 83	850	1600	160	17.8	410	0.57	0.4	9.91	11
Hirosawa 84	850	1600	160	17.8	410	1.08	0.4	8.44	11
Hirosawa 85	850	1600	160	20.8	410	1.08	0.4	8.44	9.4
Kuang U1.0	1200	1200	100	30.4	520	1.05	0.92	0	0
Kuang U1.5	1200	1800	100	34.9	520	1.05	0.92	0	0
Li LW1	2000	2000	120	40.2	382	0.5	0.5	1.4	0
Li LW2	2000	2000	120	41.6	382	0.5	0.5	1.4	5
Li LW3	2000	2000	120	34.8	382	0.5	0.5	1.4	5
Li LW4	2000	2000	120	39.8	382	0.5	0.5	1.4	0
Li LW5	2000	2000	120	35.6	382	0.5	0.5	1.4	5
Li MW1	2000	3000	120	41.2	382	0.5	0.5	1.4	5
Li MW2	2000	3000	120	39.6	382	0.5	0.5	1.4	5
Li MW3	2000	3000	120	40.3	382	0.5	0.5	1.4	5
LiC80H04	800	1600	150	65.24	501	7.2	4.24	16.2	4
LiC80H04S	800	1600	150	65.24	501	7.2	4.24	16.2	4
LiFC80B04	800	1600	150	67.52	501	7.2	4.24	16.2	4
LiFC80H04	800	1600	150	67.52	501	7.2	4.24	16.2	4
LiFC80H06	800	1600	150	67.52	501	7.2	4.24	16.2	6
LunaSW1	3050	2867	203	24.8211	461.949	0.67	0.67	0	0
LunaSW2	3050	2867	203	48.2633	434.37	1	1	0	0
LunaSW3	3050	2867	203	53.7791	434.37	0.67	0.67	0	0
LunaSW4	3050	2867	203	28.958	461.949	0.33	0.33	0	0
LunaSW5	3050	2867	203	29.6475	461.949	1	1	0	0
LunaSW6	3050	2867	203	26.2001	461.949	0.67	0.67	0	0
LunaSW7	3050	2867	203	26.2001	461.949	0.33	0.33	0	0
LunaSW8	3050	2867	203	24.1317	461.949	1.5	1.5	0	0
LunaSW9	3050	2867	203	29.6475	461.949	1.5	0.67	0	0
LunaSW10	3050	2867	203	31.7159	461.949	1.5	0.33	0	0
LunaSW11	3050	2867	203	34.4738	461.949	0.67	0.67	1.5	0
LunaSW12	3050	2867	203	34.4738	461.949	0.33	0.33	2	0

Maier S5	1180	1200	100	37.3	574	1.01	1.13	1.13	6.3
Maier S7	1180	1200	100	34.1	555	1.01	1.13	1.13	6.3
Nagib RCSW1	600	900	100	17	276	0.31	0.37	1.1	1
PilakoutasSW4	600	1200	60	36.9	550	0.39	0.5	6.86	0
PilakoutasSW5	600	1200	60	31.8	550	0.31	0.59	12.75	0
PilakoutasSW6	600	1200	60	38.6	550	0.31	0.5	6.86	0
PilakoutasSW7	600	1200	60	32	550	0.39	0.59	12.75	0
PilakoutasSW8	600	1200	60	45.8	550	0.28	0.5	7.14	0
PilakoutasSW9	600	1200	60	38.9	550	0.56	0.5	7.14	0
Salonikios LSW1	1,200	1200	100	22.2	598	0.565	0.565	1.7	0
Salonikios LSW2	1,200	1200	100	21.6	598	0.277	0.277	1.3	0
Salonikios LSW3	1,200	1200	100	23.9	598	0.277	0.277	1.3	3
Salonikios LSW4	1,200	1200	100	23.2	598	0.277	0.277	1.3	0
Salonikios LSW5	1,200	1200	100	24.9	598	0.277	0.277	1.3	0
SalonikiosMSW1	1,200	1800	100	26.1	598	0.565	0.565	1.7	0
SalonikiosMSW2	1,200	1800	100	26.2	598	0.277	0.277	1.3	0
SalonikiosMSW3	1,200	1800	100	24.1	598	0.277	0.277	1.3	3
SalonikiosMSW4	1,200	1800	100	24.6	598	0.277	0.277	1.3	0
SalonikiosMSW5	1,200	1800	100	22	598	0.277	0.277	1.3	0
SalonikiosMSW6	1,200	1800	100	27.5	598	0.565	0.565	1.7	0
Sato 36M830	2150	1400	150	39.3	296	1.16	1.16	1.16	5.1
Sato 36M850	2150	1400	150	37.5	528	0.72	0.72	0.72	5.3
Seki RB15P	3076	2020	75	28.9	381	1.2	1.2	1.2	3.5
Seki RC15P	3076	2620	75	29.2	349	1.2	1.2	1.2	3.5
Spec 1 Hidalgo	1000	2000	120	19.4	392	0.131	0.251	8.5	0
Spec 2 Hidalgo	1000	2000	120	19.6	402	0.246	0.251	8.5	0
Spec 4 Hidalgo	1000	2000	120	19.5	402	0.381	0.251	10.58	0
Spec 6 Hidalgo	1300	1800	120	17.6	314	0.131	0.259	6.54	0
Spec 7 Hidalgo	1300	1800	120	18.1	471	0.246	0.125	6.54	0
Spec 8 Hidalgo	1300	1800	120	15.7	471	0.246	0.259	6.54	0
Spec 9 Hidalgo	1300	1800	100	17.6	366	0.255	0.255	0	0
Spec 10 Hidalgo	1300	1800	80	16.4	367	0.25	0.25	0	0
Spec 11 Hidalgo	1400	1400	100	16.3	362	0.127	0.255	5.71	0
Spec 12 Hidalgo	1400	1400	100	17	366	0.255	0.127	5.71	0
Spec 13 Hidalgo	1400	1400	100	18.1	370	0.255	0.255	5.71	0
Spec 14 Hidalgo	1700	1200	80	17.1	366	0.125	0.25	4.41	0
Spec 15 Hidalgo	1700	1200	80	19	366	0.25	0.125	4.41	0
Spec 16 Hidalgo	1700	1200	80	18.8	366	0.25	0.25	4.41	0
Terzioglu T1S1	1500	750	120	23.7	481	0.34	0.34	5.15	0
Terzioglu T1S2	1500	750	120	24	584	0.34	0.34	5.15	0
Terzioglu T1N10S1	1500	750	120	27	584	0.34	0.34	5.15	10

Terzioglu T2S3	1500	750	120	29	584	0.68	0.68	5.15	0
Terzioglu T5S1	1500	1500	120	35	584	0.68	0.34	9.75	0
Terzioglu T3S1	1500	750	120	32.1	584	0.68	0.68	0.65	0
Tran S38	1219.2	2667	152.4	47.1	465	0.27	0.27	3.23	10
Tran S51	1219.2	2057.4	152.4	48.8	465	0.32	0.32	3.23	10
Tran S63	1219.2	2667	152.4	48.6	465	0.61	0.61	7.11	10
Tran S64	1219.2	2057.4	152.4	57.5	465	0.61	0.61	6.06	2.5
Tran S78	1219.2	2057.4	152.4	55.8	465	0.73	0.73	6.06	10
Vecchio DP1	3076	2020	75	21.7	605	0.76	0.82	0.37	54
Vecchio DP2	3086	2020	75	18.8	605	0.76	0.82	0.35	0

Figure 2 shows a representation of the experimental dataset shown in Table 2. As can be seen in the figure, the experimental dataset contains walls with different geometrical characteristics and design parameters. Specifically, the walls had lengths (l_w) between 600 mm and 3068 mm, heights (h_w) between 610 mm and 3000 mm, thicknesses (t_w) between 60 mm and 400 mm, concrete compressive strengths (f'_c) between 13.7 MPa and 67.52 MPa, yield strengths of reinforcement (f_y) between 276 MPa and 785 MPa, horizontal reinforcement ratios (ρ_h) between 0% and 7.2%, vertical reinforcement ratios (ρ_v) between 0.1% and 4.2%, boundary reinforcement ratios (ρ_{be}) between 0% and 16.2%, and axial load ratios (n) between 0% and 54%.

As can be seen in Figure 2, the length and height of the walls are well scattered in the dataset, while the thickness values of the walls are mainly between 100 mm and 200 mm due to the typical laboratory challenges associated with testing walls with larger thicknesses. In addition, the dataset is dominated by a large number of walls with concrete compressive strength values between 20 MPa and 40 MPa. Moreover, most of the walls have reinforcement yield strength values between 350 MPa and 600 MPa with horizontal and vertical reinforcement ratios of less than 2.5%; however, such walls have higher boundary element reinforcement ratios up to 16.2%. Also, the axial load ratios for the majority of the walls in the dataset have values between 0% and

10%. The values of these geometrical characteristics and design parameters match well those used in RC construction practice.

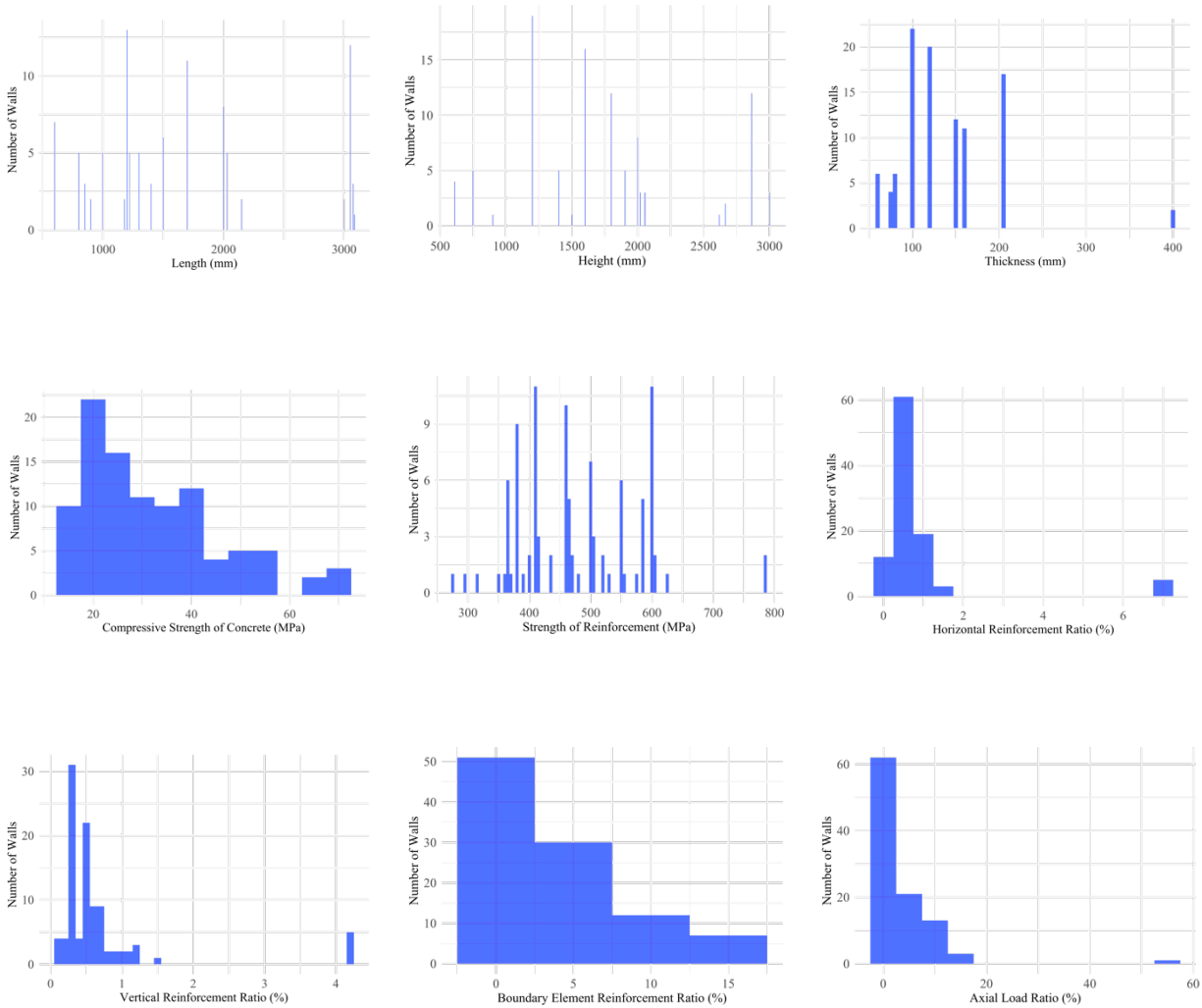


Figure 2: The Number of Squat RC Shear Walls Corresponding to their Different Geometrical Characteristics and Design Parameters

6. NSGA-II Toolbox Architecture

6.1 Background of NSGA-II

The toolbox used in the current work to predict the BWBN model parameters utilizes multi-objective optimization (MO) and evolutionary algorithms (EA). The toolbox was originally

developed by Deb et al. (2002) based on the NSGA-II algorithm. The algorithm minimizes the following four objectives simultaneously to achieve a solution:

- The Manhattan distance between the displacements obtained from the lab ($x(t)$) and the displacements ($\hat{x}(t|p)$) predicted with the BWBN model of hysteresis:

$$f_1(p) = \sum_{i=1}^n \frac{|x(t_i) - \hat{x}(t_i|p)|}{\omega(t_i)}$$

Equation 15

The Manhattan distance is modified to include a vector $w(t)$, a weighting function, which contains data used to normalize the displacements between $[-1,1]$. This vector is computed using the displacement records by a method that allows linear interpolation between the ultimate values of the absolute displacement values. This procedure is performed to provide small and large displacements with the same significance to create a normalized set of data.

- The uniform norm (infinity norm) of the error between the displacements measured at the lab ($x(t)$) and the predicted displacements ($\hat{x}(t|p)$):

$$f_2(p) = \max_{1 \leq i \leq n} \{|x(t_i) - \hat{x}(t_i|p)|\}$$

Equation 16

Minimizing this function allows for better results by providing an improved approximation of the displacements field, thus making the hysteresis loops well-suited and adjusted.

- The difference between the total dissipated energy calculated using the load-displacement records (ε_{tot}), and the total dissipated energy obtained from the BWBN model of hysteresis ($\varepsilon_{tot}|p$):

$$f_3(p) = |\varepsilon_{tot} - \varepsilon_{tot}|p|$$

Equation 17

It is imperative to know that the total dissipated energy is the summation of the hysteretic dissipated energy and the elastic dissipated energy. The total dissipated energy is denoted by the area encompassed by the hysteresis curves, hence minimizing the above equation reveals a good approximation of the estimated hysteresis cycles regarding the shape of the experimental hysteresis loops.

- The uniform norm (infinity norm) of the error between the dissipated energy computed from records ($\varepsilon_{tot}(t)$) and the predicted dissipated energy ($\varepsilon_{tot}(t|p)$):

$$f_4(p) = \max_{1 \leq i \leq n} \{|\varepsilon_{tot}(t_i) - \varepsilon_{tot}(t_i|p)|\}$$

Equation 18

In order to ensure that each hysteretic cycle is well approximated, minimizing this objective is essential. The reason is that the total dissipated energy is a cumulative measure, and the dissipated energy is minimized during the time frame history. Furthermore, during an earthquake, it is crucial for the system to discharge gained energy to allow for the structure to remain serviceable.

6.2 BWBN Parameters Using NSGA-II

The power of the NSGA-II toolbox is utilized in the current thesis to process and evaluate the dataset collected for squat RC shear walls. Some of the inputs used in the toolbox are the population size, number of generations, mass of the system, the initial stiffness of the system, and the number of registries recorded at the lab. Table 3 presents the BWBN parameters that are quantified based on the dataset, offering insights that span across various wall properties and their respective responses. This toolbox, renowned for its advanced multi-objective optimization capabilities, proved instrumental in deciphering the intricate patterns and underlying correlations present within previous datasets (Yusoff, Ngadiman, & Zain 2011). Therefore, by employing the NSGA-II, the goal is to achieve a comprehensive understanding of each shear wall's characteristics

and then develop specific BWBN model parameters that are pivotal for their subsequent hysteretic responses. The details of these parameters, which have been meticulously deduced using the toolbox, are shown in Tables 4 and 5. This endeavour underscores the significance of adopting sophisticated computational tools in structural engineering studies, as they provide a more holistic and accurate portrayal of the subject matter.

Table 3. The BWBN Parameters Used in the NSGA-II Toolbox

Wall Parameter	Description
ξ	Damping Ratio
α	Post-Yield to Pre-Yield Stiffness Ratio
β	Bouc-Wen Model Co-effi. (Beta)
γ	Bouc-Wen Model Co-effi. (Gamma)
n	Hardening-Softening Parameter
ν_0	Strength Degradation
$\delta\nu$	Strength Degradation Parameter
A_0	Hysteresis Amplitude
δA	Control Parameter for Amplitude in terms of Energy
η_0	Stiffness Degradation
$\delta\eta$	Stiffness Degradation Parameter
p	Initial Pinching Controller
νs_0	Pinching Severity
ψ_0	Pinching Parameter
$\delta\psi$	Change of Pinching Controller
λ	Pinching Parameter (Lambda)
q	Pinching Parameter (q)

Table 4. The BWBN Parameter Values for the 100 Squat RC Shear Walls Based on the NSGA-II Toolbox

Wall ID	ξ	α	β	γ	n	ν_0	$\delta\nu$	A_0
Beko 1	0.1585215	0.2763636	0.3942286	-0.351255	1.014955	0.1072989	0.006823293	2.551414
Beko 4	0.06773931	0.2283581	1.03233	-0.2680038	1.006078	0.1011723	0.01388621	2.941386
ChengH115	0.1964445	0.2553308	1.383558	-1.298013	1.08064	0.1513842	0.01072743	1.284991
ChengH60	0.1934821	0.2488744	0.1884814	-0.1627925	1.190225	0.5101534	0.01582026	1.873577
ChengH60X	0.1483348	0.02876748	1.889114	-1.73535	1.001681	0.1001761	0.003892664	2.673118

ChengM115	0.1427276	0.0769642	1.265428	-1.247076	1.183067	0.1056388	0.158419	2.929641
ChengM60	0.1094953	0.2031263	0.6295875	-0.5630986	1.006537	0.1426584	0.1183702	2.719528
Greifenhagen M1	0.1395516	0.2763494	0.5796345	-0.3722843	1.111332	0.1086136	0.4871412	2.616934
Greifenhagen M2	0.07661674	0.1660005	0.4016275	0.01141368	1.000325	0.1512542	0.6340387	2.241432
Greifenhagen M3	0.1909963	0.1086624	0.180233	0.4626158	1.251971	0.7574301	0.03121582	2.031202
Greifenhagen M4	0.1960318	0.09891394	0.6847279	-0.1257833	1.483514	0.301862	0.3510252	1.827341
Hirosawa 72	0.1861946	0.1616883	0.1565409	-0.1342786	1.040605	0.1055522	0.6833485	2.918956
Hirosawa 73	0.1970954	0.2635218	0.834745	-0.5688319	1.001364	0.282913	0.1948651	2.815817
Hirosawa 74	0.04756883	0.2842993	0.4390376	-0.407287	1.088656	0.1034849	0.2191448	2.969716
Hirosawa 75	0.1779526	0.2048127	0.3773382	-0.3616958	1.083688	0.1188056	0.4589617	2.893988
Hirosawa 76	0.1717406	0.1115952	0.105063	-0.0889764	1.009549	0.146196	1.138797	2.980616
Hirosawa 77	0.1141672	0.2930243	0.1023153	-0.09766465	1.048242	0.1267841	1.600738	2.825111
Hirosawa 80	0.02179907	0.2402754	0.2136281	0.4770603	1.004924	0.1209145	0.1921575	2.999409
Hirosawa 81	0.1959483	0.2592438	0.387329	-0.1862771	1.099551	0.100997	0.392176	2.901356
Hirosawa 83	0.1960974	0.1014014	0.3357013	-0.1078082	1.003649	0.1011609	0.4376979	2.613902
Hirosawa 84	0.08442994	0.1607177	0.8634223	0.007678749	1.453714	0.2909879	0.144186	0.1141153
Hirosawa 85	0.03416466	0.1007391	0.5807947	-0.2591783	1.02189	0.1128264	0.3931881	2.723254
Kuang U1.0	0.1988016	0.2572836	0.7849821	-0.5871275	1.201297	0.1017427	0.1533779	2.91881
Kuang U1.5	0.07647547	0.06610868	0.5330448	-0.4161047	1.005456	0.3067978	0.2315502	1.323561
Li LW1	0.1850359	0.208245	0.352006	-0.2626476	1.106454	0.3264116	0.6074959	2.394456
Li LW2	0.1155087	0.2035102	0.5265115	-0.3751564	1.019827	0.1227634	0.1817036	2.504484
Li LW3	0.1804458	0.2913933	0.367478	-0.2879285	1.064981	0.6245656	0.2775886	2.922017
Li LW4	0.1321356	0.1474282	1.046434	-0.979059	1.067233	0.1771859	0.2356827	2.83787
Li LW5	0.1383141	0.257582	0.7000698	-0.6816073	1.019966	0.1115699	0.4710194	1.856455
Li MW1	0.1416262	0.1304407	1.828177	-1,790,072	1.000312	0.1141813	0.8858363	2.972852
Li MW2	0.191236	0.176664	0.8687794	-0.8516432	1.110625	0.2550095	0.2280411	2.943907
Li MW3	0.191236	0.176664	0.8687794	-0.8516432	1.110625	0.2550096	0.2280411	2.943907

LiC80H04	0.1731524	0.1677814	0.8887849	-0.7946258	1.034905	0.2259378	0.2041709	2.51437
LiC80H04S	0.1938958	0.1201084	0.1237951	-0.09047414	1.008013	0.02338953	0.264058	2.739997
LiFC80B04	0.1961461	0.233599	0.10547	0.007483268	1.019493	0.3466309	0.2613637	2.898973
LiFC80H04	0.1981984	0.155219	0.1715222	-0.1377975	1.0076685	0.1068388	0.2616897	2.914533
LiFC80H06	0.1617485	0.1456082	1.261017	-1.248826	1.043789	0.1114959	0.3137922	2.995536
LunaSW1	0.1616955	0.04133738	0.7788639	-0.6431267	1.004102	0.1978748	0.2739052	2.520439
LunaSW2	0.1917884	0.2898128	0.5009621	-0.41478	1.18521	0.1422902	0.05093526	2.125872
LunaSW3	0.092831	0.2371751	3.03436	-2.953142	1.00445	0.1161279	0.02931076	2.692606
LunaSW4	0.1868815	0.2941245	1.322274	-1.284896	1.085132	0.105855	0.1223241	2.669566
LunaSW5	0.1238033	0.2877346	0.1603736	0.2769761	1.026649	0.1005436	0.01944897	2.100707
LunaSW6	0.1901663	0.2676738	0.1003143	-0.00775376	1.065122	0.1041371	0.01852847	2,844,204
LunaSW7	0.1675847	0.2529292	0.3142068	-0.23555474	1.061088	0.1404926	0.009765611	2.774886
LunaSW8	0.138317	0.1917654	1.148063	-0.9806038	1.005859	0.1104987	0.02219037	2.441293
LunaSW9	0.1238033	0.2877346	0.1603736	0.2769761	1.026649	0.1005436	0.01944897	2.100707
LunaSW10	0.19202023	0.2981914	0.2098977	-0.0701923	1.00247	0.1245187	0.01914279	2.66651
LunaSW11	0.179284	0.290835	0.1975966	-0.1683191	1.000398	0.2974219	0.1641787	2.509635
LunaSW12	0.11504	0.2998992	1.275633	-1.247565	1.007265	0.3511059	0.01220532	2.84806
Maier S5	0.05852465	0.299313	0.1071423	0.1617598	1.02583	0.119688	0.2510441	2.933988
Maier S7	0.08105137	0.2790898	0.3153229	0.4917827	1.191693	0.2430978	0.00654305	2.919192
Nagib RCSW1	0.1839419	0.061123	0.4809222	-0.3787267	1.041128	1.528439	1.254808	1.51036
PilakoutasSW4	0.1984936	0.03627199	0.7167278	-0.5095583	1.236583	0.6076541	0.1818918	2.150102
PilakoutasSW5	0.1367	0.02699438	0.6072995	0.3453473	1.321027	0.2016373	0.3600922	0.5545764
PilakoutasSW6	0.1877476	0.06842177	0.6437808	-0.4151993	1.105276	0.1079178	0.317683	1.711431
PilakoutasSW7	0.1791096	0.1159234	0.3040582	-0.1250785	1.115571	0.1019871	0.495414	1.442002
PilakoutasSW8	0.176545	0.03875565	0.6635192	-0.6173806	1.189479	0.4411328	0.1924109	1.893101
PilakoutasSW9	0.1714925	0.02425626	0.7054221	-0.698233	1.461234	0.1296657	0.165692	1.588379
Salonikios LSW1	0.1724296	0.2138134	0.3826611	-0.1822423	1.01169	0.2539202	0.4810751	2.94127

Salonikios LSW2	0.05972412	0.09656338	5.470557	-1.347312	1.036558	0.05399055	0.8383841	1.60418
Salonikios LSW3	0.1990844	0.1859405	0.2681128	-0.1516186	1.006035	0.1046071	0.3672337	2.795149
Salonikios LSW4	0.1859338	0.1968343	0.992057	-0.4636506	1.137064	0.1156643	0.1780813	2.957093
Salonikios LSW5	0.1639353	0.1561736	0.3142722	-0.1339626	1.191265	0.1119553	0.3610658	2.978705
SalonikiosMSW1	0.1724296	0.2138134	0.3826611	-0.1822423	1.01169	0.2539202	0.4810751	2.94127
SalonikiosMSW2	0.09136761	0.02295022	0.94256	-0.9272962	1.330463	0.5572252	0.3291879	1.530865
SalonikiosMSW3	0.1990844	0.1859405	0.2681128	-0.1516186	1.006035	0.1046071	0.3672337	2.795149
SalonikiosMSW4	0.1513487	0.01646768	0.8857747	-0.7352325	1.22459	0.3936043	0.2727366	2.272964
SalonikiosMSW5	0.1533805	0.03885438	1.827495	-1.708998	1.015996	0.3373452	0.1872253	2.799244
SalonikiosMSW6	0.1433366	0.04191794	0.1204517	-0.1115159	1.115118	0.1349796	0.7561169	1.614583
Sato 36M830	0.1817989	0.1711003	0.1316861	0.009494815	1.078424	0.1017513	0.1223747	2.894017
Sato 36M850	0.08096248	0.2997424	0.3958022	-0.01387612	1.009476	0.1089946	0.04767618	2.993085
Seki RB15P	0.08873979	0.2752752	0.3196971	-0.2988183	1.040157	0.1071732	0.09773359	2.613639
Seki RC15P	0.1982648	0.04541951	0.5151225	-0.4330574	1.042293	0.1034946	0.07463774	2.640502
Spec 1 Hidalgo	0.1752859	0.00902923	0.6264039	-0.6135239	1.122047	1.828638	0.6934984	2.777243
Spec 2 Hidalgo	0.1952348	0.09557039	1.080931	-0.9863381	1.215544	0.2781012	0.1515286	2.917316
Spec 4 Hidalgo	0.1871878	0.08930638	1.046901	-1.0104	1.024875	0.2517215	0.0824535	2.995598
Spec 6 Hidalgo	0.1736562	0.1325473	0.7088991	-0.6452423	1.007326	0.4231381	0.1795171	2.995303
Spec 7 Hidalgo	0.1653804	0.1964917	0.5301714	-0.517677	1.002027	0.3536609	0.3857669	2.959358
Spec 8 Hidalgo	0.1607392	0.2380827	0.7110802	-0.63067	1.109217	0.3015558	0.4931421	2.22499
Spec 9 Hidalgo	0.1968045	0.1201426	0.6099966	-0.6011354	1.0559	0.3394124	0.3226613	2.302499
Spec 10 Hidalgo	0.1987974	0.1617983	0.1966513	-0.1566648	1.040562	0.198359	2.227568	2.69719
Spec 11 Hidalgo	0.4725719	0.1581381	0.4872661	-0.4770752	1.63778	0.1062251	0.7444747	2.869894
Spec 12 Hidalgo	0.1678931	0.2952876	0.8368285	-0.6797639	1.230064	0.1089064	0.6205634	2.989425
Spec 13 Hidalgo	0.0903034	0.1571561	0.060930221	-0.3474603	1.050977	0.1050607	0.5100079	2.881393
Spec 14 Hidalgo	0.1863882	0.2447419	0.1315245	-0.1018645	1.024698	0.1009216	1.81262	2.962716
Spec 15 Hidalgo	0.03748069	0.299527	0.1866728	-0.1545412	1.123313	0.1251715	1.195719	2.609097

Spec 16 Hidalgo	0.02443206	0.1512678	0.2517321	-0.05596517	1.004784	0.1570009	0.5044465	2.972069
Terzioglu T1S1	0.03721683	0.01300116	0.7666152	0.8653264	1.03333	0.1797523	0.2242002	2.65314
Terzioglu T1S2	0.1973097	0.05947773	0.7173845	-0.02157558	1.155868	0.1751602	0.05237519	1.750417
Terzioglu T1N10S1	0.040513	0.2940981	0.4948829	0.4948809	1.021771	0.09803256	0.1262455	2.346117
Terzioglu T2S3	0.02067557	0.09784726	0.5031944	0.008699195	1.000916	0.1007457	0.2203532	2.875079
Terzioglu T5S1	0.1881811	0.05857662	1.162882	-0.1994835	1.01385	0.1018719	0.05355153	1.632069
Terzioglu T3S1	0.1959754	0.03363297	1.510254	0.4443119	1.069662	0.04049895	0.08298119	2.316324
Tran S38	0.1261016	0.01870754	0.778805	-0.6720285	1.172176	0.6468976	0.1902289	2.667195
Tran S51	0.1997673	0.12285	0.1331066	-0.06318224	1.020312	0.1788839	0.2926182	2.976356
Tran S63	0.1751985	0.07533869	0.9310891	-0.9233899	1.16779	0.1868209	0.5337902	2.9396
Tran S64	0.02330441	0.01551941	1.598463	-1.580195	1.111703	0.4766096	0.3049534	2.835962
Tran S78	0.1975815	0.03405153	1.291369	-1.27036	1.023013	0.1676221	0.2676658	2.765745
Vecchio DP1	0.1886175	0.2804782	0.6700382	-0.6199607	1.004183	0.1028467	0.01658604	2.994472
Vecchio DP2	0.1024214	0.2407497	0.3969637	-0.2685458	1.052398	0.1397932	0.04163464	2.852022

Table 5. The BWBN Parameter Values for the 100 Squat RC Shear Walls Based on the NSGA-II Toolbox

Wall ID	deltaA	eta0	deltaeta	p	vs0	psi0	deltapsi	lambda	q
Beko 1	-9.184665	0.1182141	0.63491	4.577865	1.003445	-1.843459	-0.7419678	2.238892	3.852808
Beko 4	-9.67559	0.1479251	0.6837414	2.5973	-1.048273	3.588957	-1.184262	-2.531292	3.587548
ChengH115	-1.968596	0.3856248	0.3820478	0.2000154	1.735562	-2.574995	0.1101797	-1.067749	3.576856
ChengH60	-1.904559	0.2331443	0.26085	8.933973	0.962676	-0.6500528	2.447382	-1.009072	3.158964
ChengH60X	-1.817604	0.1528985	2.841339	1.212184	-5.313521	1.256416	3.812638	0.7231068	1.470161
ChengM115	-1.922365	0.9045746	1.848936	7.893072	2.013231	-0.2266153	0.03657749	-1.222517	0.718438
ChengM60	-1.66964	0.2409422	0.8693889	1.42847	1.431048	-3.241898	0.2092111	-1.034797	3.795763
Greifenhagen M1	-0.6349939	3.907126	3.583215	4.84966	-2.936288	-3.701976	-2.041739	3.151638	3.686605
Greifenhagen M2	-0.07496651	2.698495	1.399109	0.06379808	-4.155067	0.08054107	0.2412748	1.945925	3.236184
Greifenhagen M3	-1.981944	3.192935	3.577534	1.09415	2.309437	0.5784469	0.1309579	-1.397121	9.393972
Greifenhagen M4	-1.471939	3.440888	3.745654	0.2948873	0.9626274	0.5094907	0.05383469	-0.6994068	2.350879

Hirosawa 72	-1.010319	0.3301303	1.18283	5.247612	-3.041722	0.4768081	1.142208	2.904833	-3.515606
Hirosawa 73	-1.147973	0.5362312	1.217865	9.120849	-1.900319	-2.162882	0.2553572	-3.265399	1.622279
Hirosawa 74	-0.9850285	0.333834	0.753583	0.8302999	-1.173749	1.955837	2.690595	1.24497	-2.200584
Hirosawa 75	-1.941255	0.5510373	1.647555	1.543796	0.9416695	-2.743445	-2.140706	-1.235012	2.671235
Hirosawa 76	-0.6424951	0.424835	0.7205432	7.597541	0.57596	-0.779041	-0.3203658	-1.918696	3.300177
Hirosawa 77	-1.351114	0.5355806	1.16481	0.2369137	0.6765574	2.611813	3.491571	-0.3672454	2.367132
Hirosawa 80	-1.370157	0.9269635	1.112961	3.4467	-2.219745	-1.170652	0.1842114	0.2599269	3.958148
Hirosawa 81	-0.8802494	0.3325317	1.36743	3.433601	-2.11826	-2.734338	0.4117965	0.8186415	2.203534
Hirosawa 83	-0.2399516	2.863713	1.343656	3.925867	-3.233651	-1.706633	-0.1680621	2.563	-3.956965
Hirosawa 84	-0.568412	4.615335	5.01484	1.249707	0.7882644	2.025945	2.06564	2.416564	-1.541059
Hirosawa 85	-0.6296089	1.485659	2.830932	0.6490419	-1.036688	0.6583167	-0.0625867	3.547254	2.157736
Kuang U1.0	-1.982546	1.36507	1.8473	4.847655	0.9278576	-2.160189	0.9973975	-0.7893251	2.215136
Kuang U1.5	-0.00474022	3.913553	3.120804	0.0466527	-2.167136	-0.0235117	1.797494	3.184544	3.499268
Li LW1	-0.08683763	0.7686046	1.155448	0.5659989	-1.485067	0.8430181	3.17563	-3.225513	3.426002
Li LW2	-0.3321218	0.3714113	0.6984353	4.578631	0.5936445	3.913891	-3.843298	0.1985219	-2.986865
Li LW3	-0.9920525	0.4542274	1.353302	0.4346561	0.4898168	-0.5919151	0.8799694	-1.039472	2.419259
Li LW4	0.01987834	1.26855	1.462735	0.9782329	-0.803458	2.070457	2.457312	0.3421617	0.8806808
Li LW5	-1.838627	2.005163	2.602843	7.143431	0.936861	3.647772	-0.4923451	-0.05798684	0.7199779
Li MW1	0.07076133	2.122349	2.484078	1.965136	-1.130044	-0.5741926	3.467085	2.886859	1.433233
Li MW2	0.1722441	2.189381	1.649874	7.954279	-0.614073	-2.851528	1.867942	-1.499472	0.1932205
Li MW3	0.1722441	2.189381	1.639874	7.954279	0.6140731	-2.851528	1.867942	-1.499472	0.1932205
LiC80H04	-0.9943917	1.971733	3.316041	6.636551	1.974518	2.666988	-0.1059696	-2.231549	3.042003
LiC80H04S	-0.01613686	1.94718	0.8141189	1.038738	-2.515815	-1.558395	-0.032317	3.411678	0.910381
LiFC80B04	-0.0934857	2.813453	0.6348683	0.0313511	-5.217204	2.245184	0.6384177	1.607426	1.871278
LiFC80H04	-0.02961235	1.910005	0.2436929	3.248664	3.231695	1.692155	-0.031787	-3.100391	3.044901
LiFC80H06	-1.259925	1.703796	3.111237	5.040267	0.905401	3.406224	-0.6008921	-0.7871645	2.939473
LunaSW1	-1.248921	0.2426401	1.510249	1.833399	0.8081117	3.19321	-0.9516847	0.005248814	-2.903406
LunaSW2	-1.658023	1.45865	3.651814	8.250534	-7.846491	2.968735	2.778456	-3.227922	0.2140703
LunaSW3	-1.935003	1.118485	0.9448264	0.2075012	1.258163	-3.449436	0.1668165	-0.9069585	1.088725
LunaSW4	-1.256535	0.2293853	0.8511857	1.765123	0.9430547	2.267954	-0.4120443	-1.40151	0.5704631
LunaSW5	-1.848112	1.289911	1.011374	7.469364	-7.473661	-2.784527	-3.202109	-3.922589	0.9175608
LunaSW6	-1.839441	0.4665783	0.4858878	1.606934	0.9481445	1.780843	1.094006	-1.77048	1.512455

LunaSW7	-1.960509	1.00864	0.6756647	7.596118	1.456026	-1.572931	0.227357	-1.813327	2.028189
LunaSW8	-1.87388	0.1779434	0.6135481	5.423096	0.9966361	-3.776158	1.015313	-1.037981	1.187204
LunaSW9	-1.848112	1.289911	1.011374	7.469364	-7.473661	-2.784527	-3.202109	-3.922589	0.9175608
LunaSW10	-1.924886	0.7193607	0.4738701	6.400613	0.9112804	-3.921247	0.5423616	-2.606345	1.38854
LunaSW11	-1.731031	0.3442856	0.4322965	2.116469	2.092089	-3.359667	-0.9603947	-2.022009	2.914869
LunaSW12	-1.915468	0.4405643	0.4593997	9.73802	0.8070247	0.1426084	0.1565291	3.981637	0.8274835
Maier S5	-10.52708	1.274914	1.630489	9.845782	-1.183973	1.289643	3.728079	-2.796575	1.029828
Maier S7	-1.956812	1.321428	1.013372	8.292007	-0.541716	0.8746736	-1.753893	-2.879148	1.647759
Nagib RCSW1	-1.751328	3.245749	7.709145	0.0749541	1.610311	-0.410668	-0.2727978	-1.876888	6.988827
PilakoutasSW4	-0.0542494	3.403763	3.294563	1.177212	-1.012915	0.5677304	-0.7134337	0.3195586	0.6556881
PilakoutasSW5	-1.601562	3.642332	3.223462	4.098161	0.9932131	-0.7753749	0.1715103	-1.073698	2.992922
PilakoutasSW6	-0.01839851	3.613586	2.581668	0.00479907	-7.866084	0.7409806	-0.2551806	1.109308	1.813692
PilakoutasSW7	-0.03032912	3.463199	1.747391	4.932731	-4.29713	-0.4347665	-0.0475663	2.795388	3.2284
PilakoutasSW8	0.007913427	3.250523	1.401842	6.987417	-2.480975	2.036432	2.933367	2.359056	-3.495044
PilakoutasSW9	-0.00685988	3.430292	1.207702	4.85973	-0.7845532	-2.260339	-0.4463483	-2.394281	-2.124206
Salonikios LSW1	-0.4117765	1.47188	0.9927067	0.9849861	0.9514497	-3.12519	0.4236889	-0.8405785	2.284774
Salonikios LSW2	-0.268354	3.345655	0.9965337	8.687746	-0.1205396	1.129967	-3.10957	-1.869099	2.630179
Salonikios LSW3	-0.0228838	1.952857	0.1738303	2.973235	-3.18098	-0.8665008	-0.6559953	3.251732	1.012971
Salonikios LSW4	-0.02254959	1.451496	1.082565	9.970604	-2.935009	-1.285717	0.6737529	2.05853	3.249241
Salonikios LSW5	-0.04552502	1.970653	0.3655459	0.8732286	-1.612487	1.085881	-0.275433	1.304648	2.269349
SalonikiosMSW1	-0.4117765	1.47188	0.9927067	0.9849861	0.9514497	-3.12519	0.4236889	-0.8405785	2.284774
SalonikiosMSW2	0.01413314	3.564862	3.717338	1.827414	-1.518806	-0.1976408	-2.290488	3.044642	0.7334733
SalonikiosMSW3	-0.0228838	1.952857	0.1738303	2.973235	-3.18098	-0.8665008	-0.6559953	3.251732	1.012971
SalonikiosMSW4	-0.05147905	3.965525	3.500235	5.287753	-1.529995	-1.370976	-0.8833049	0.5988069	1.233579
SalonikiosMSW5	0.01259703	3.391955	2.538216	0.2527402	-2.38541	-0.2938169	2.630218	-3.408286	-3.977649
SalonikiosMSW6	0.02874814	3.416088	0.7485084	8.235642	-0.616113	-0.1624202	-0.2414044	-3.616309	3.496612
Sato 36M830	-1.689636	0.5516871	2.005089	1.745577	-4.80463	-1.679137	-3.638123	-3.736638	0.2514091
Sato 36M850	-1.765223	0.3448219	2.082899	6.130632	-4.81829	-2.101487	-3.627875	-2.97452	1.2661
Seki RB15P	-1.997515	0.3259759	0.5482051	7.775641	0.691327	1.613231	1.223507	0.1911152	2.106368
Seki RC15P	-1.594055	0.3709733	0.9353946	7.907252	0.3951215	1.635645	-0.529798	-2.237694	1.497649
Spec 1 Hidalgo	0.05143661	2.455572	2.385573	4.888132	-3.962095	-3.978198	-0.4449156	2.644566	-1.723096
Spec 2 Hidalgo	0.07014976	3.993248	1.549427	7.095367	-1.619606	-1.260653	0.5906663	1.948671	0.4888502

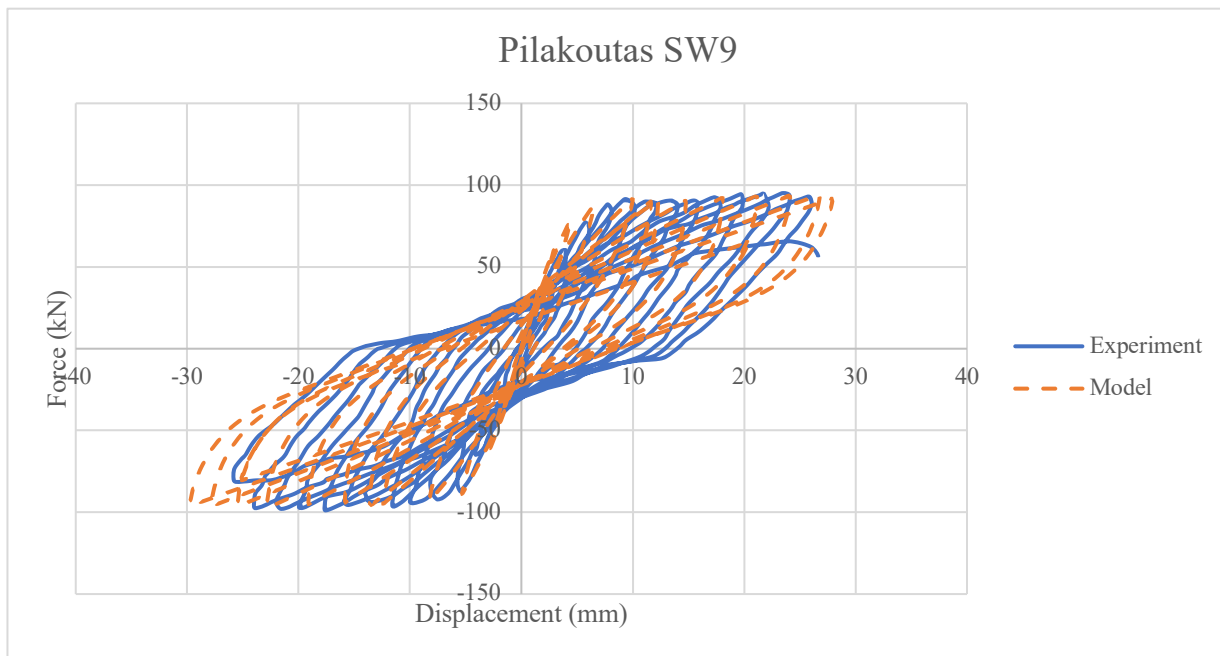
Spec 4 Hidalgo	0.09076878	1.831051	1.289826	1.859804	-4.229243	-2.63961	-2.858646	3.634524	-1.366042
Spec 6 Hidalgo	0.07507666	0.8331452	2.571835	8.657991	-1.543203	-3.128486	3.326767	-0.3227987	3.243059
Spec 7 Hidalgo	0.04859122	0.8530637	1.266056	6.901546	-1.833652	-1.429269	1.171748	-3.999462	0.4611575
Spec 8 Hidalgo	-1.365451	1.203813	3.456396	6.771497	1.015734	-2.234808	0.8515695	-0.9884104	1.490343
Spec 9 Hidalgo	-0.01589937	1.237096	0.9891337	5.050442	0.629537	-3.77996	0.7217815	1.755503	1.731083
Spec 10 Hidalgo	0.1131874	3.678501	3.269718	0.5202389	-5.298474	3.971009	-1.646699	3.950561	3.978316
Spec 11 Hidalgo	0.004937263	1.295735	2.575146	3.977074	-0.4698413	-1.177515	-1.159811	-0.6656334	0.3799409
Spec 12 Hidalgo	-1.637222	1.048907	2.796571	7.065989	1.025961	1.689225	0.1080632	-0.9700555	1.925459
Spec 13 Hidalgo	-1.843313	1.174283	2.0283	1.365867	0.9567374	0.8639878	-0.9418702	-1.083999	1.885617
Spec 14 Hidalgo	0.212905	1.226561	0.7681123	8.487747	-2.61887	-0.5485575	-1.227081	-0.7334907	9.669482
Spec 15 Hidalgo	-1.878366	0.9491844	1.569472	8.669807	1.674813	-0.0802746	-0.1156423	-1.496627	0.933163
Spec 16 Hidalgo	-1.49151	1.36785	0.7807805	4.0889	0.7988183	-2.995808	-0.6292708	-1.063685	2.691654
Terzioglu T1S1	-12.22279	1.368045	7.154201	4.404423	0.9925203	-0.308646	1.192897	-1.022694	4.608458
Terzioglu T1S2	-3.571037	1.942854	3.544655	8.172425	0.9904874	-0.9409396	-1.233554	-0.9719192	2.49289
Terzioglu TIN10S1	-19.44953	0.9473295	7.799584	0.1442941	1.008031	3.056992	0.4338919	-1.082996	6.894905
Terzioglu T2S3	-15.46102	1.860236	8.864532	7.463059	0.969682	1.046289	0.222283	-1.099867	6.422969
Terzioglu T5S1	-4.723877	1.561466	4.190457	9.853995	0.982675	-1.163102	0.1844774	-0.8263447	7.534353
Terzioglu T3S1	-9.428836	1.384706	9.486516	8.254242	0.9820821	-0.5397463	0.9964651	-1.035217	2.39203
Tran S38	-0.2561104	1.727154	0.8016819	0.06291508	0.761425	-3.940135	2.121901	0.6644544	-1.986401
Tran S51	-0.06342832	2.217476	0.2822492	2.121373	-4.023945	3.547934	2.596732	-0.14087	2.824142
Tran S63	-1.695055	3.92544	2.55041	0.04550478	0.9836777	-3.627418	1.004963	-1.01447	3.249442
Tran S64	-4.246113	1.166089	6.416734	0.01853163	1.45116	1.575725	-0.0560898	-1.197306	1.351391
Tran S78	-1.459214	1.102189	3.083734	6.851324	0.9911283	3.025633	-0.1158894	-1.040871	2.127921
Vecchio DP1	-1.996551	0.4469668	0.6289076	0.218268	0.6492665	-3.936789	0.2588669	-2.262943	0.3581511
Vecchio DP2	-1.28141	0.5459223	0.6464153	2.21045	-4.461777	-1.31768	0.2059174	-0.4455051	-2.735699

6.3 Hysteretic Behaviour Validation

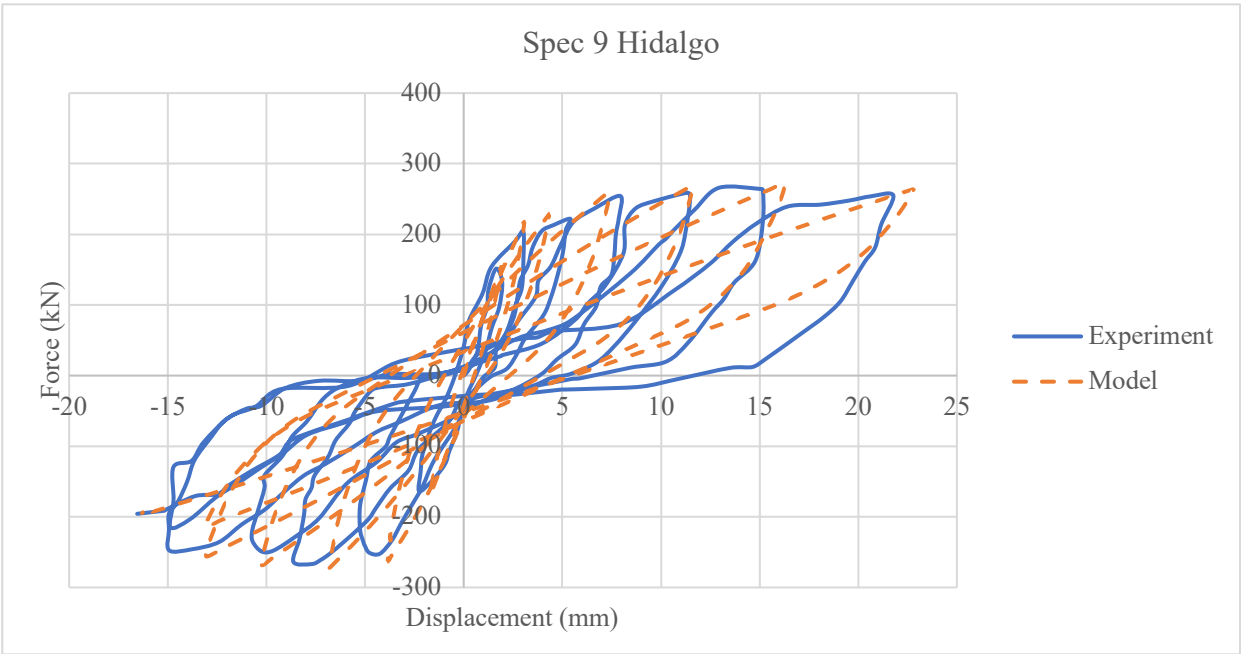
The NSGA-II toolbox was used to estimate the BWN model parameters and then establish the hysteretic relationship for each wall within the dataset. The experimental results of each wall were compared to the results obtained from the NSGA-II algorithm. This step was crucial to validate

the estimated parameters of each wall and its subsequent hysteretic response relative to the experimental counterpart, as shown in Figures 3a to 3e, for five walls that were tested by Pilakoutas et al. (1995), Li et al. (2011), Hidalgo et al. (2002), Salonikios et al. (2005), and Kuang et al. (2008). As can be seen in the figure, the NSGA-II algorithm through the estimated BWBN parameters is able to predict the experimental hysteretic responses of such walls to a great extent. For example, for wall SW9 by Pilakoutas et al. (1995), the maximum experimental restoring force and displacement are 98.46 kN and 25.84 mm, respectively, while the NSGA-II algorithm shows values of 97.04 kN and 29.76 mm for the same two parameters, respectively.

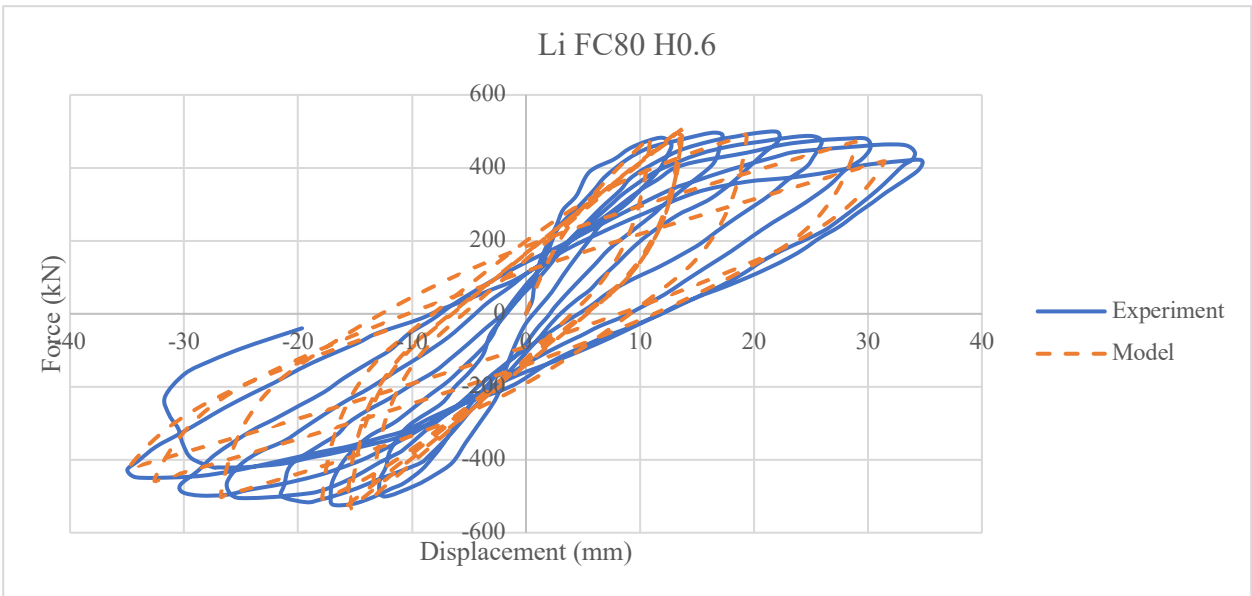
a)



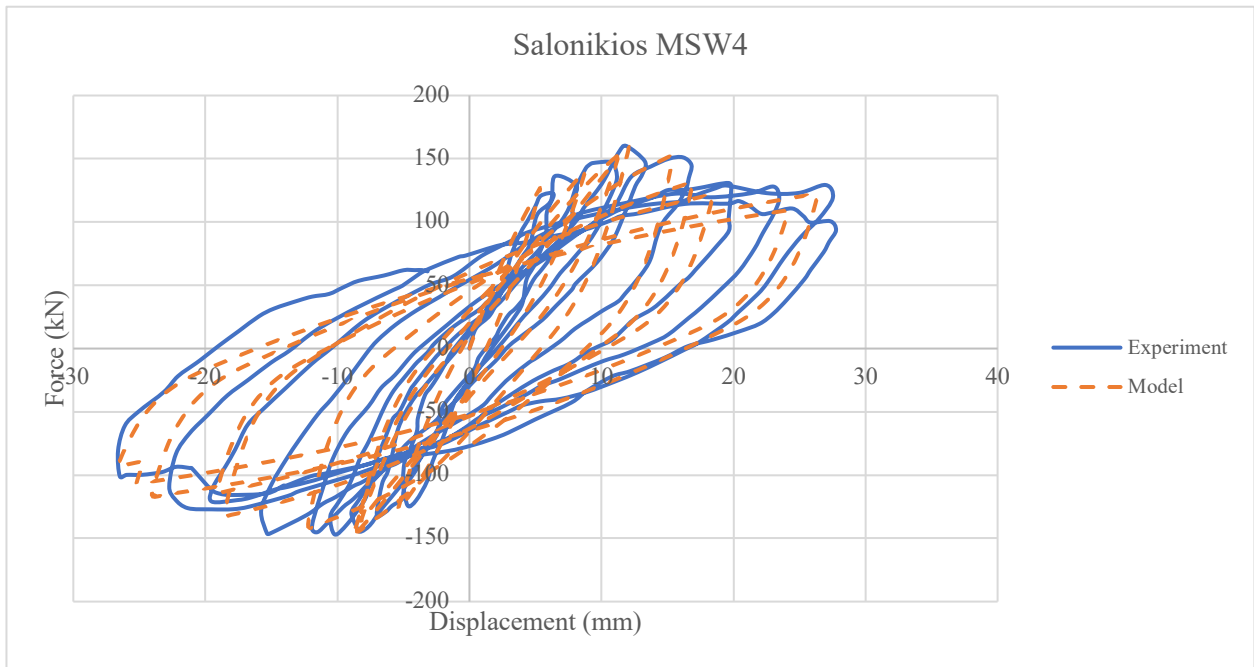
b)



c)



d)



e)

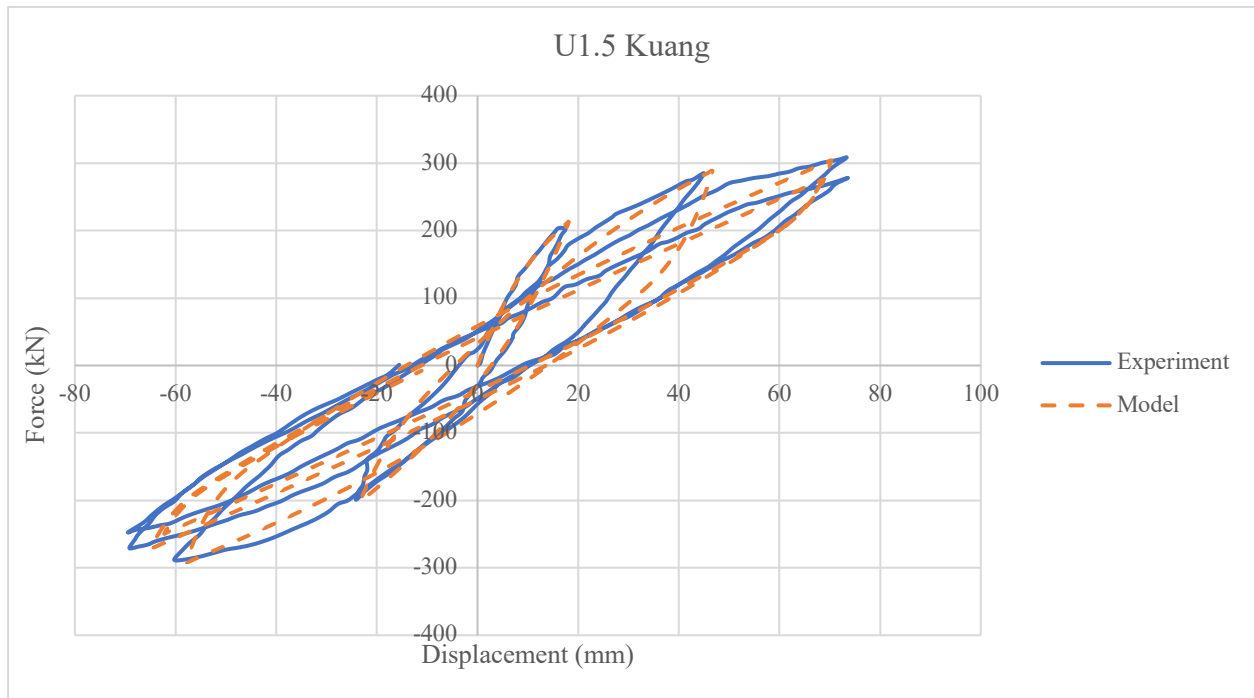


Figure 3: Experimental versus NSGA-II Results for Different Squat RC Shear Walls

7. Data Management

Exploratory Data Analysis (EDA) serves as a foundational pillar in the analytical realm, offering a preliminary perspective through which datasets can be deciphered. This analysis ensures that any subsequent detailed investigations are anchored on a foundation that is free of inconsistencies or biases (Mao 2015). By weaving together statistical summaries and graphical interpretations, EDA illuminates the core characteristics of datasets. In the context of the current thesis on squat RC shear walls, EDA can shed light on the intricate attributes intrinsic to the dataset.

7.1 Data Cleaning and Transformation

The initial phase encompasses data cleaning and transformation. This step was of paramount importance, as it entailed preprocessing the data to address missing experimental values and establish consistency across all the wall parameters. Given the vast and varied nature of the squat RC shear wall dataset, meticulously curating and then refining the data were also crucial to eliminate potential inaccuracies and noise. Furthermore, one of the pivotal phases was outlier detection. Given the extensive scope of the dataset, it was imperative to meticulously identify and address any anomalies. Therefore, observations that significantly deviated from established norms underwent rigorous scrutiny, ensuring the robustness and integrity of all subsequent analyses.

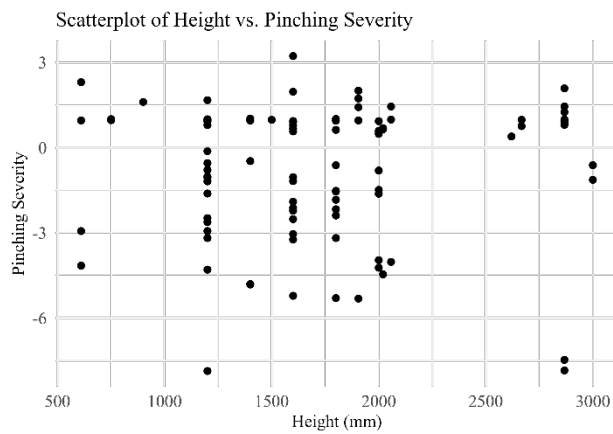
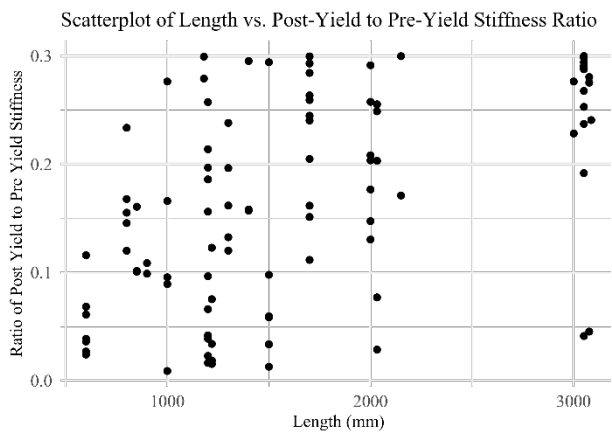
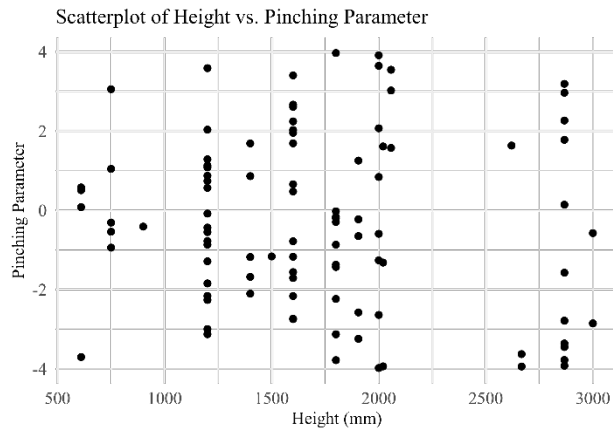
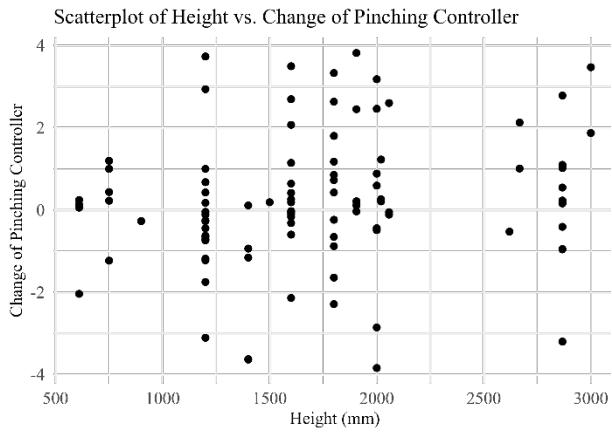
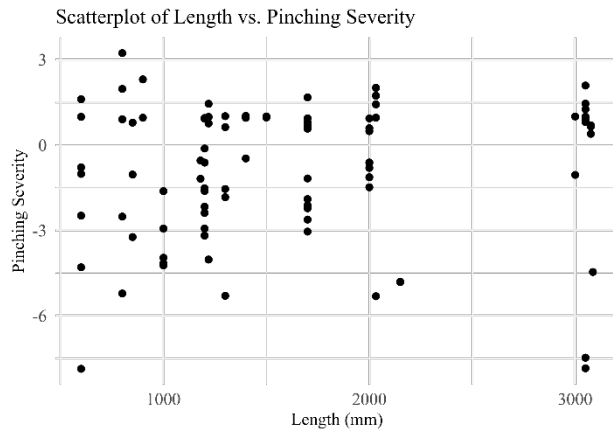
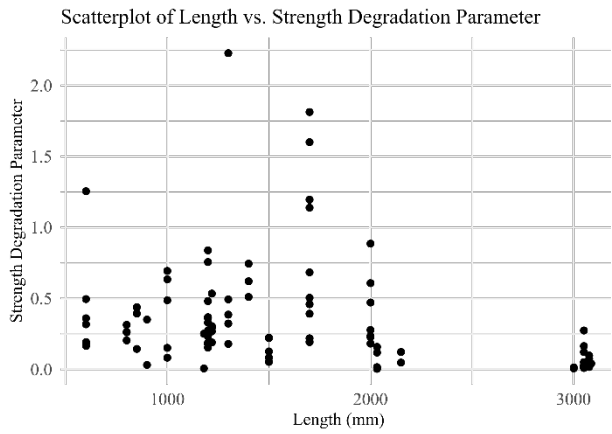
7.2 Data Visualization

The following step in the data management was to visualize the data. Using a diverse array of visualization tools, from histograms (i.e., as shown earlier in Figure 2) that present delineating distribution of wall parameters to scatterplots that underscore relationships between the various BWBN and wall parameters, a more nuanced understanding of the dataset can be achieved. These visual explorations, coupled with the insights derived from the NSGA-II toolbox, offer a

comprehensive visual narrative of the data. Additionally, descriptive statistics further augment this narrative.

Scatterplots serve as a pivotal graphical representation in data analysis, providing a clear visual assessment of the potential relationships between variables. The individual points plotted on this two-dimensional graph crystallize the joint distribution of the data, unveiling patterns, trends, and correlations that might not be apparent in tabulated numerical data. Notably, scatterplots can reveal the subtleties of data interrelations, whether linear or nonlinear, and aid in identifying outliers that could signify anomalies or errors in data collection. They are indispensable for preliminary exploratory analysis, as they assist in formulating hypotheses about causal relationships and can guide the researcher in selecting appropriate statistical tests. In essence, scatterplots do not just depict data; they narrate a story, revealing the character and dynamics of the variables under scrutiny, thus forming an essential foundational tool in the thesis narrative.

Figure 4 shows scatterplot examples of the relationships between the various BWBN and wall parameters. As can be seen in the figure, the scatterplot for the relationship between the length and strength degradation of the walls shows some dominant regions where values cluster. Specifically, walls with a length of roughly 3000 mm exhibit strength degradation parameter values between 0 and 0.5, and similarly, walls with a length of about 2000 mm show a wider range of strength degradation parameter values ranging from 0 to 1. Appendix A contains all the scatterplots developed during the current work to visually understand all the underlying relationships. The results in this figure and all other figures in Appendix A clearly demonstrate that the BWBN parameter values and subsequently the hysteretic response of the walls rely on more than one geometrical characteristic of such walls.



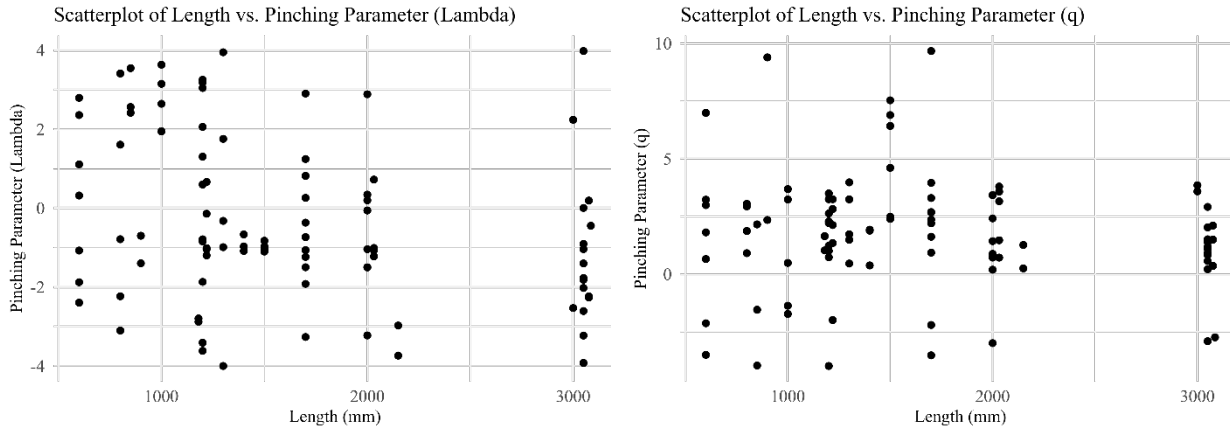


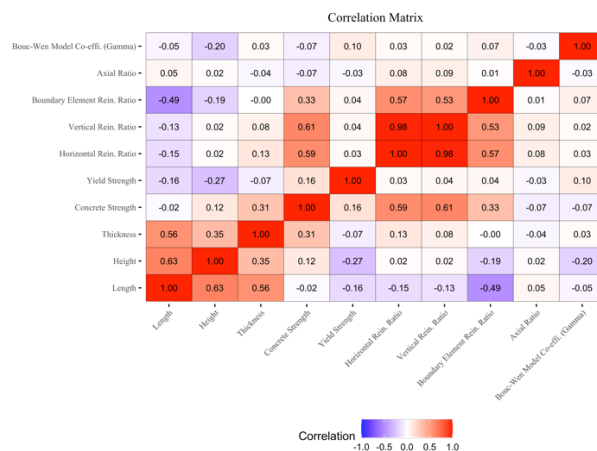
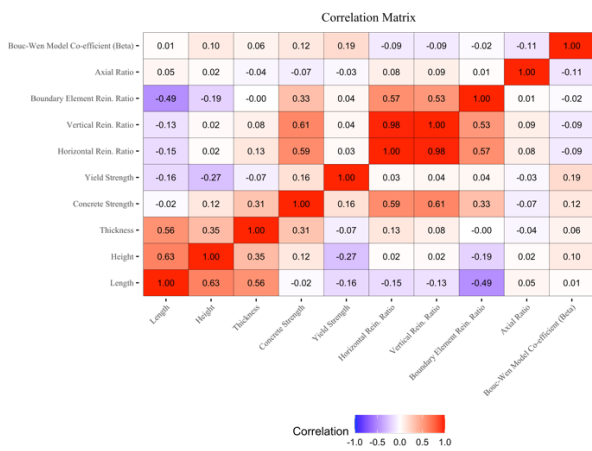
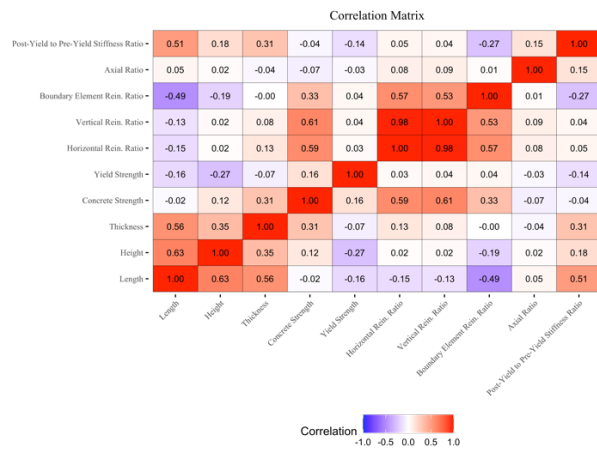
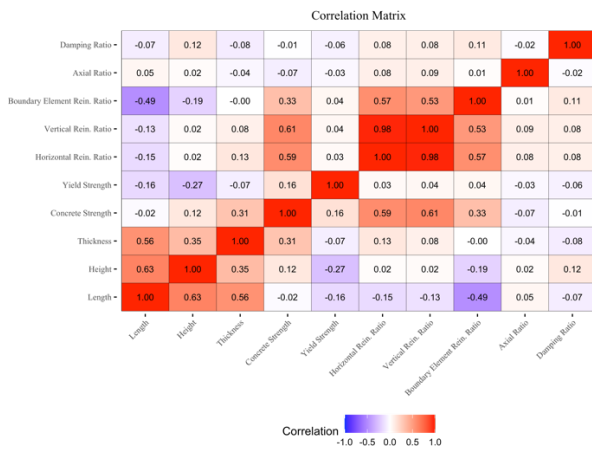
Figure 4: Scatterplots of Squat RC Shear Walls Corresponding to Different Parameters

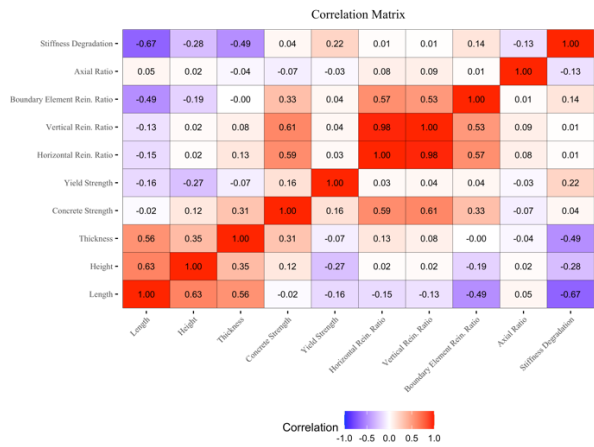
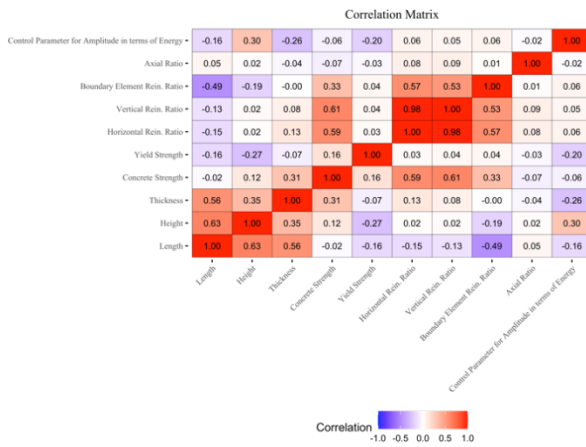
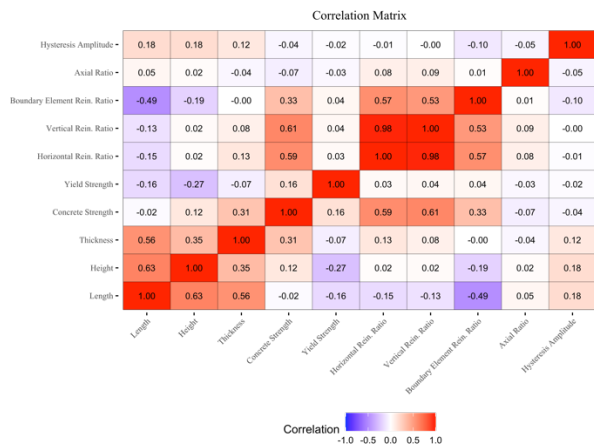
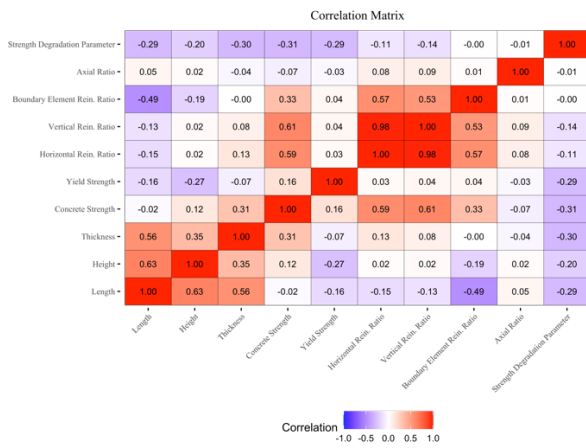
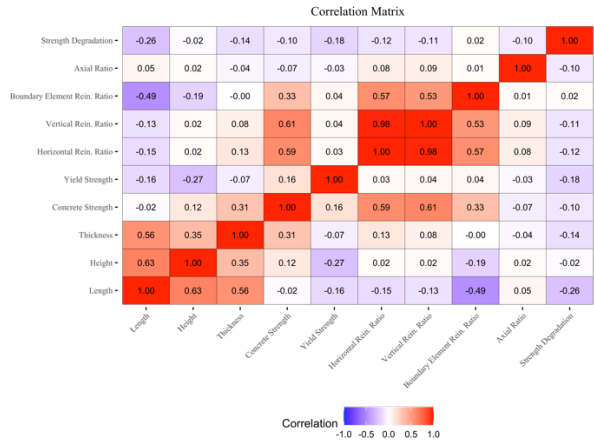
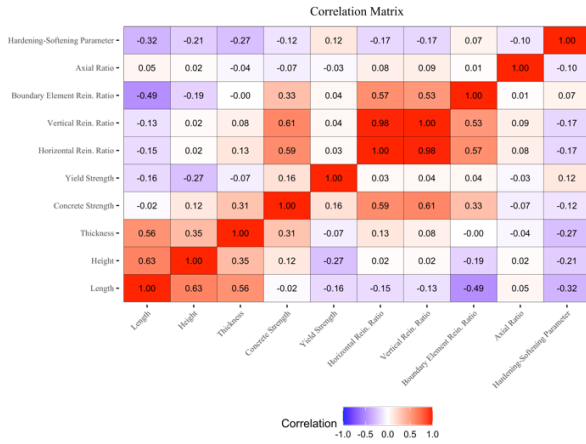
7.3 Correlation Analysis

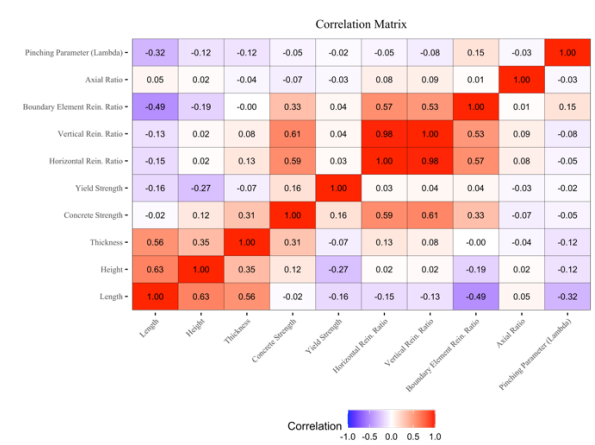
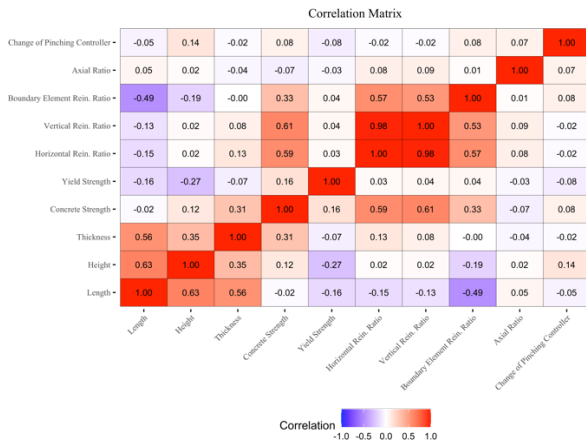
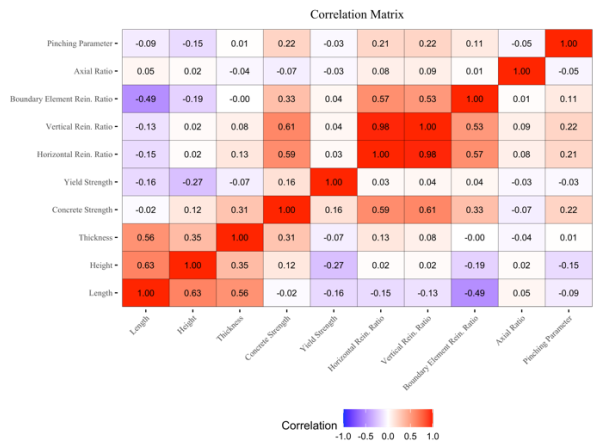
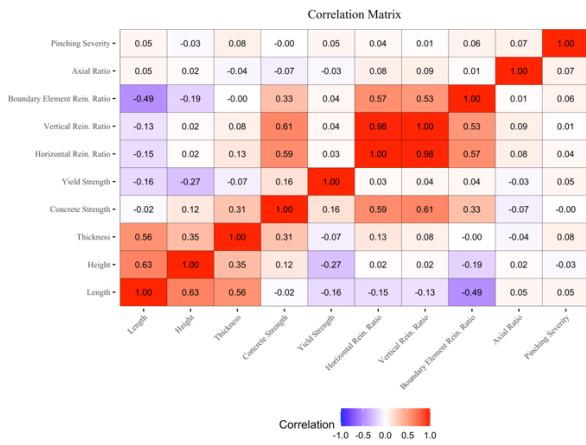
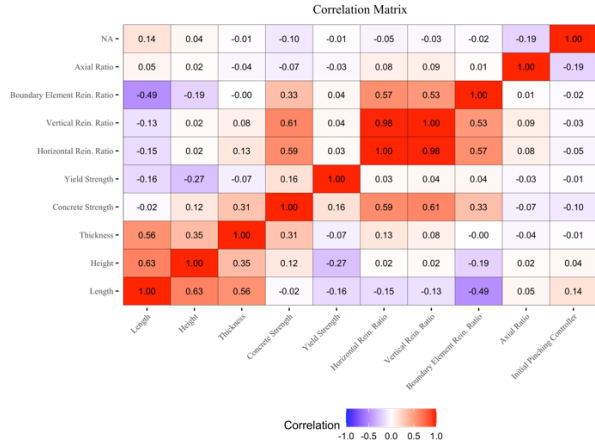
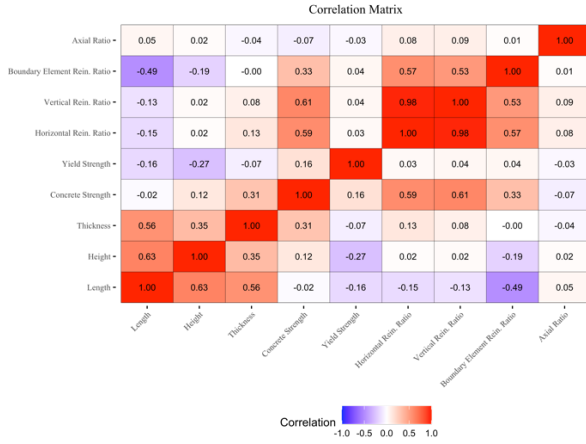
Correlation analysis is a statistical method used to examine the relationship between two or more variables. The goal of correlation analysis is to determine the strength and direction of the relationship between the variables and to identify any patterns or trends that exist between them. There are two main types of correlation analysis: Pearson's correlation and Spearman's rank correlation. Pearson's correlation measures the linear relationship between two continuous variables and is expressed as a value between -1 and 1. A value of 1 indicates a perfect positive linear relationship, meaning that as one variable increases, the other variable increases at a constant rate. A value of -1 indicates a perfect negative linear relationship, meaning that as one variable increases, the other variable decreases at a constant rate. A value of 0 indicates that there is no linear relationship between the variables. Spearman's rank correlation is used to measure the relationship between two ordinal or ranked variables. It is also expressed as a value between -1 and 1, with a value of 1 indicating a perfect positive relationship and a value of -1 indicating a perfect negative relationship.

Both Pearson's correlation and Spearman's rank correlation can be used to test the hypothesis that there is some type of relationship between the variables. The data visualization was performed

using R-language and Pearson's method for determining correlation amongst variables was used. This is performed by calculating a p-value, which is the probability of observing the observed correlation by chance if there is no relationship between the variables. If the p-value is less than a certain significance level, such as 0.05, then the hypothesis of no relationship is rejected, and it is concluded that there is a significant correlation between the variables. Figure 5 shows correlation matrices between the wall parameters and each BWN parameter.







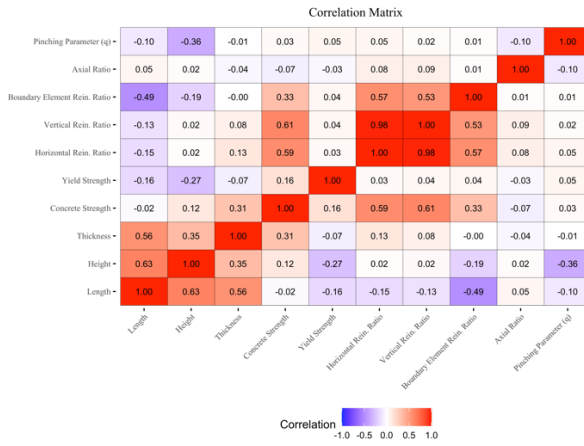


Figure 5: Correlation Matrices for the Different Wall and BWN Parameters

According to the correlation matrices shown above, it is clearly visible that each BWBN parameter is related to the wall’s descriptive parameter. For example, the damping ratio is positively correlated to the height and all reinforcement ratios, whereas it is negatively correlated to the length, thickness, concrete strength and yield strength. These relationships are very useful when establishing a preliminary outlook on the fitness function for each BWBN variable.

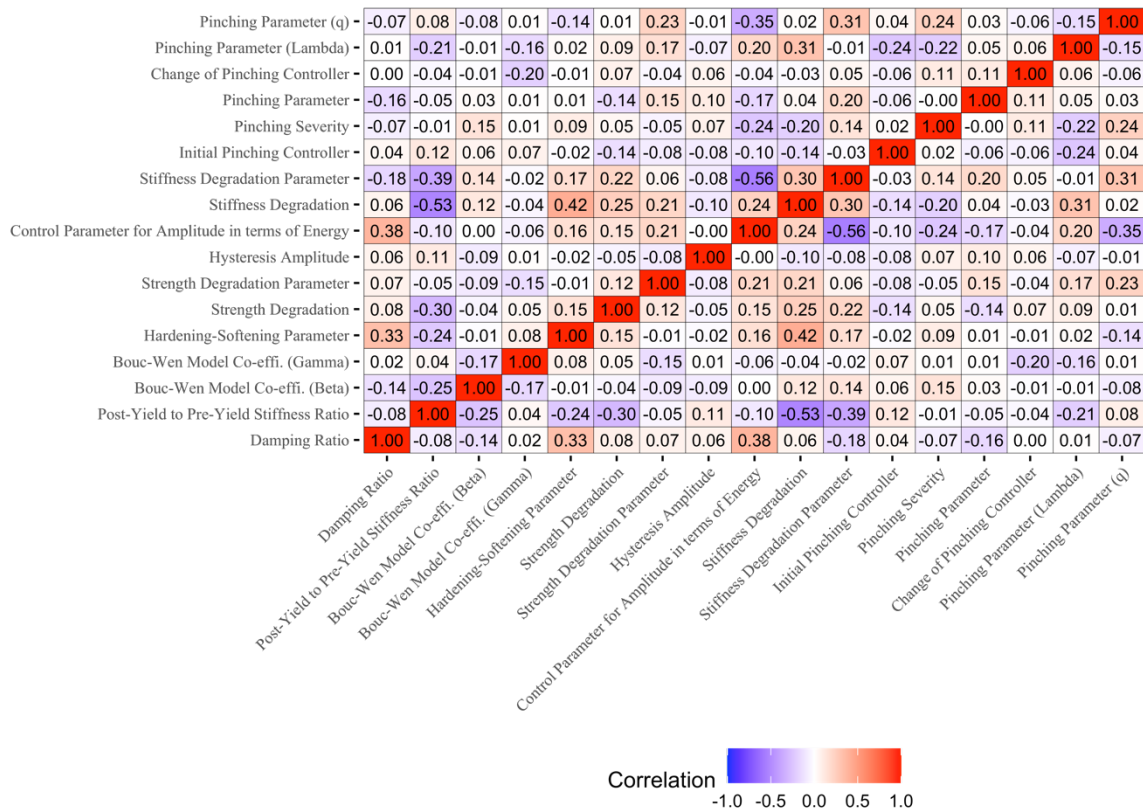


Figure 6: A Correlation Matrix for the Different BWBN Parameters

Figure 6 shows the correlation matrix for all the BWBN parameters amongst each other. As shown in the figure, most of the BWBN parameters are not significantly related to each other, which is crucial for the current work as it demonstrates that including all the BWBN parameters to quantify the hysteretic response of the walls is key for accurate predictions. However, it is also important to understand some of the parameters are more positively and negatively correlated with

each other in comparison with the rest of the parameters. For example, the stiffness degradation parameter and the control parameter for amplitude in terms of energy are negatively correlated with a value of -0.56. Conversely, the highest positively correlated parameters are the stiffness degradation and hardening-softening parameters with a value of 0.42. This correlation makes sense since stiffness degradation and hardening-softening parameters are intrinsically linked facets of structural behaviour under stress. Stiffness degradation chronicles the loss of a wall's rigidity, while hardening or softening illuminates the change in a wall's strength post-yield. These parameters are vital in the design phase, where they inform the anticipated performance of RC walls under dynamic loading conditions. Together, they paint a comprehensive picture of structural integrity, guiding engineers in optimizing designs for both safety and durability. Their interdependence is particularly crucial in seismic design, where they contribute to a structure's ability to withstand and dissipate energy during seismic events.

8. Genetic Programming

As observed through a vast expanse of preceding studies, there is an undeniable and urgent need to evolve and lean towards methodologies that are deeply rooted in advanced, data-driven approaches. This urgency is precisely where genetic programming (GP) finds its calling. Tracing back to its conceptual origins, it was Koza (1992) who laid the cornerstone for GP, drawing rich inspirations from the intricate Darwinian theory of evolution. As time progressed, GP burgeoned into a potent evolutionary computing algorithm, further solidifying its position within the realms of artificial intelligence. This evolution and its capabilities have been diligently noted and documented by Ashour et al. (2003).

One of the many facets that make GP a standout is its inherent proficiency. It not only effortlessly models the often-perplexing non-linear relationships that are rooted in historical

datasets but is also known for its unmatched ability to yield actionable design interpretations. A plethora of scholarly works, including insightful contributions from Pérez et al. (2012), Cladera et al. (2014), Kara (2011), and Yosry et al. (2019), emphasize the distinct edge GP has over traditional model prediction (MP) techniques and even many of the modern machine learning paradigms.

Perhaps, the most pronounced advantage of GP, especially when juxtaposed against conventional PM techniques, is its unparalleled freedom from reliance on specific model structures. Often, these structures, like mechanical pointers, are designed to mimic certain system phenomena. With GP, there's an emancipation from the need for prior, in-depth knowledge of the intricate nuances of the system's physical, mechanical, or geometrical attributes. GP uniquely utilizes symbolic regression. It embarks on a comprehensive journey, scanning and sifting through every conceivable function-variable combination, with its compass guided solely by the input dataset. This exhaustive search persists until it identifies and refines an optimal model that best resonates with the data, a notion extensively detailed by Pérez et al. (2012).

Acting as an anchor in heuristic optimization, GP exhibits a commendable prowess in optimizing symbolic regression searches, as emphasized by Cladera et al. (2014). Being an evolutionary computational beast, GP continually refines and enhances its approach, guiding the predictive model search in a highly intelligent manner. This iterative refinement method effectively sidelines a vast multitude of suboptimal model variations, a process that Kara (2011) eloquently sheds light upon. When positioned against the myriad of machine learning techniques available today, GP stands tall, primarily due to its unmatched capacity to generate crystalline, precise expressions. These expressions seamlessly bridge the system's input variables to the sought-after output, a phenomenon captured in the works of both Geem et al. (2001) and Cladera

et al. (2014). These lucid, programmable expressions serve as beacons, helping researchers and practitioners alike to dissect and grasp the often-elusive behaviours exhibited by multifaceted systems, such as the shear resistance mechanisms frequently associated with SRCSW-BE.

However, even with its myriad of undeniable advantages and strengths, the broader adoption of GP within the structural engineering landscape remains somewhat limited. A relatively scant number of studies have explored its depth, with a few venturing into the shear strength of RC beams endowed with stirrup reinforcement, as documented by Ashour et al. (2003), Perez et al. (2012), Cladera et al. (2014), and Gandomi et al. (2017). Additional research frontiers include deep RC beams (Gandomi et al. 2013), composite beams (Köroğlu et al. 2011), short rectangular RC columns (Aval et al. 2017), structures with fibre polymers (Kara 2011; Nehdi et al. 2007), and RC shear walls (Gondia et al. 2020).

8.1 Genetic Programming Procedure

GP, as a computational strategy, derives its foundational ethos from the evolutionary tenets delineated by Charles Darwin (1859). Embedded within the realm of heuristic optimization, GP, with its proven acumen in symbolic regression, facilitates the extraction of precise, nearly optimal expressions that accurately represent the intricacies of multifaceted systems (Cladera et al. 2014). Referring to the depicted process (in Figure 7) obtained from (Gondia, Ezzeldin, & El-Dakhakhni, 2020), a collection of P entities (termed individuals) commences with an initial grouping (referred to as a population) and undergoes propagation across N generational phases. Throughout these phases, the population is subjected to evolutionary mechanisms such as elitism, mutation, and crossover. These processes systematically refine the population, leading to the emergence of an optimized entity of substantial precision by the final generation, as per the methodologies outlined by Koza (1992) and Cladera et al. (2014).

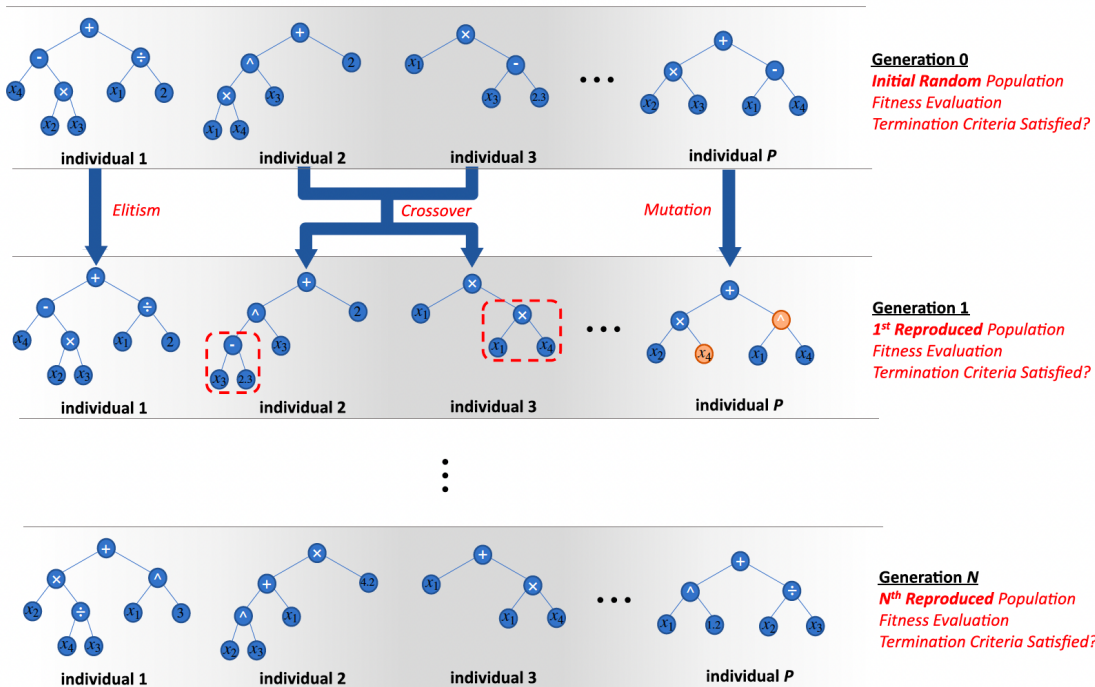


Figure 7: Evolutions of GP Individuals (Expressions) throughout Generations

The procedural intricacies of GP are represented using an expression and are systematically organized within tree architectures, as exemplified in Figure 8 (Ashour et al. 2003; Gondia et al. 2020). Intricately designed, these trees encompass terminal nodes, representative of preordained input variables and constants, juxtaposed with non-terminal nodes, which epitomize functional operations. Collectively, these nodes coalesce, crafting mathematical expressions of significance (Cladera et al. 2014). Prior to the activation of the GP algorithm, a meticulous configuration of these nodal entities is imperative, as it pre-determines the tree's evolution trajectory. For a holistic comprehension, Figure 9, as conceptualized by Koza (1992), provides an elucidative flowchart, spotlighting the systematic generation of expressions within GP, adept at modelling complex system dynamics.

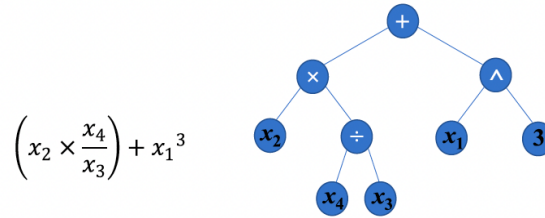


Figure 8: Example of GP Individual Represented as a Mathematical Expression and a Corresponding Tree-Shaped Structure

The overarching GP methodology, delineated in Figure 9, can be compartmentalized into four pivotal phases, corroborated by a constellation of seminal contributions, including but not limited to Koza (1992), Ashour et al. (2003), and Cladera et al. (2014):

1. Initialization Phase: An ensemble of tree-structured entities emerges from a randomized process, each emblematic of potential predictive expressions, specifically attuned to discern the hysteretic parameters of SSW. These entities manifest diverse characteristics in terms of their structural depth, configuration, and inherent complexity.
2. Evaluation Phase: Incorporating a predefined training set, the fitness quotient of each entity is rigorously evaluated. This evaluation, tethered to a bespoke fitness function, gauges the predictive efficacy of an expression. Entities demonstrating superior fitness quotients are predisposed to supersede their less competent counterparts in ensuing generations.
3. Evolutionary Dynamics Phase: This phase unfolds over a series of iterative sub-steps, each imbuing genetic operations that echo the nuances of natural evolution: elitism, crossover, and mutation. This cyclical progression perseveres until a predetermined termination criterion – which might pivot around parameters like a stipulated generation count, computational duration, or a fitness benchmark – is actualized.
4. Conclusion and Extraction Phase: Upon attainment of the termination criterion, the GP algorithm concludes its iterative journey. The fittest entity, emerging from the preceding

generation, is heralded as the quintessential solution. This solution, simultaneously portrayed as a coding tree and a deciphered mathematical construct, holds the promise of astutely predicting the hysteresis parameters intrinsic to SSW.

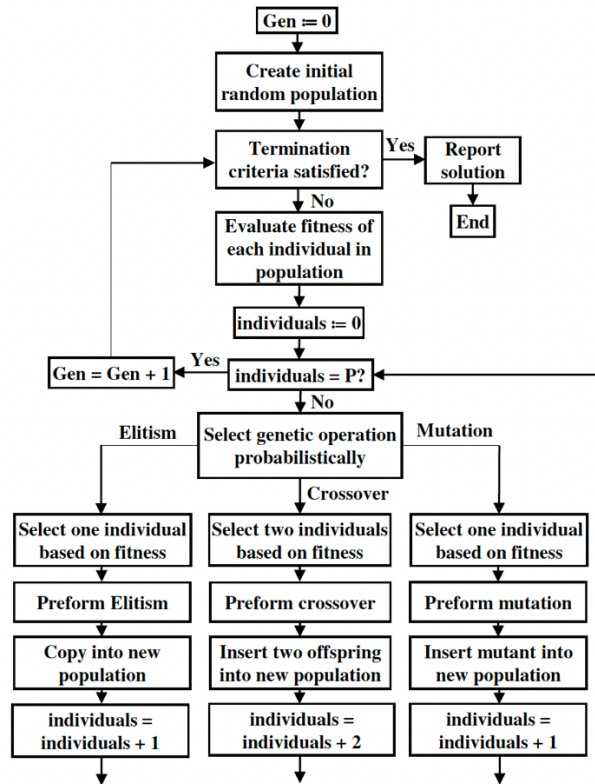


Figure 9: Flowchart Representation of GP Procedure Based on the Study by Koza (1992)

A salient feature accentuating the efficacy of GP is its polygenic disposition. Foregoing the convention of endorsing a singular tree as the definitive system solution, GP innovatively amalgamates the most competent trees from the antecedent generation. Through the meticulous application of non-linear regression (NLR), the attainment of optimal tree coefficients is realized, bolstering the overall fitness profile of the population. A pre-emptive determination of tree depth, conjoined with the polygenic methodology, eschews the emergence of overtly convoluted trees, thus preserving the elegance and simplicity of the resultant model. This synthesized model, an

ensemble in its essence, amalgamates a multitude of streamlined sub-models, each proficiently encapsulating the inherent complexity and non-linearity of the system (Safari and Mehr 2018).

8.2 Genetic Programming Utilization and Results

In the endeavour to derive complex equations for output variables in structural engineering through GP, the Distributed Evolutionary Algorithms in Python (DEAP) toolbox emerges as a pivotal instrument. DEAP is an open-source library that provides a versatile framework for the implementation of various evolutionary algorithms, including GP. It is designed with flexibility in mind, allowing researchers and engineers to tailor evolutionary strategies to their specific needs. The toolbox supports a wide range of evolutionary computation techniques, from basic genetic algorithms to more sophisticated multi-objective optimization, thereby serving as a comprehensive platform for evolutionary computation in Python. By utilizing DEAP, engineers can efficiently explore and evolve mathematical expressions that model the intricate behaviours of structural systems, leveraging the library's capabilities to perform symbolic regression, optimization, and search tasks within the GP framework.

The application of DEAP in deriving equations for structural engineering variables signifies a methodical approach to tackling the complexity of modelling structural behaviours. Through DEAP, the GP process is streamlined, enabling the efficient generation, evolution, and refinement of predictive models. The toolbox's architecture facilitates the creation of complex, tree-structured expressions that embody the relationships between various structural parameters and their impact on performance metrics. This is achieved by exploiting DEAP's genetic operators to mutate, crossover, and select the most promising models across generations, guided by a fitness function that quantifies the accuracy and relevance of the mathematical expressions to the structural phenomena being studied. Thus, DEAP not only enhances the capability to unearth novel

and accurate equations for output variables but also exemplifies the integration of advanced computational tools in engineering research, pushing the boundaries of what can be achieved in predictive modelling and design optimization.

The following equations display the relationship between the input and the output variables mentioned in the current work. The equations shown below use some or all wall parameters to help predict the corresponding BWBN variable. The DEAP toolbox can artificially select which variables will yield the best equation based on its inherent machine learning capabilities. Furthermore, the equations use some or all input variables based on the output variable selected and it is displayed throughout other equations mentioned below that help predict, for example, Post-Yield to Pre-Yield Stiffness Ratio, Bouc-Wen Model Co-effi. (Beta), and Bouc-Wen Model Co-effi. (Gamma).

The foray into utilizing GP to decipher the complex equations governing structural behaviour yielded results that necessitate careful consideration. The training Mean Squared Error (MSE) indicates the average squared difference between the predicted and actual values during the model learning phase, and the testing MSE provides a measure of predictive accuracy when the model is applied to unseen data. In the current work, the best equation derived from the GP process yielded large MSE values that were deemed not acceptable. These large values underscore the intricate challenge posed by accurately modelling such complex systems. The discrepancy between the training and testing MSE values reveals also the nuanced intricacy of the structural behaviour and the difficulty of capturing all the influencing factors within a model. As such, it is evident that future studies should further verify the effectiveness of GP to develop equations for the BWBN parameters when more experimental results for squat RC shear walls under quasi-static loading

become available. Such studies can also explore more advanced or alternative modelling techniques that can handle the multi-dimensional nature of the data more effectively.

Future research could pivot towards integrating deep learning algorithms, which are renowned for their ability to manage large-scale, complex data. The potential for neural networks to learn and model non-linear relationships could prove invaluable in reducing MSE and improving model reliability. Ensemble methods could also be harnessed to amalgamate multiple models, potentially offsetting individual model biases and variances, and leading to a more robust aggregate model. The exploration of such alternatives will be crucial in advancing the modelling techniques used in the field of structural engineering, ensuring that predictive models not only achieve lower error metrics but also resonate more faithfully with the intricate realities they aim to replicate.

$$\gamma = \left(\frac{\cos\left(\frac{\cos(\rho_h + n)}{\rho_h + 0.404 \times \sin(fc)}\right)}{(\rho_h + 0.404 \times \sin(fc))(\rho_h + n)(\sin^3(tw) + n)n} \right)$$

Equation 22

$$\nu_0 = 0.272 \times \cos\left(\sin\left(0.791 + \frac{0.791 + \frac{0.167}{lw} + \frac{0.167}{lw}}{lw} + \rho_h\right)\right)$$

Equation 23

$$\delta\nu = 0.336$$

$$\begin{aligned} & \cdot \cos(lw) \\ & \cdot \sin(\sin(\rho_v - tw)) \\ & \cdot \sin(\sin(\sin(tw) \cdot \cos(0.3362)) \cdot \sin(\rho_v - tw) \cdot \sin(tw) \cdot \cos(0.336)) - tw) \\ & \cdot \sin(tw) \cdot \cos(0.336)) \end{aligned}$$

Equation 24

$$\begin{aligned} A_0 &= \frac{A}{\sin(\rho_v)} \cdot 1 \\ & / \left(\cos\left(\frac{(2tw + \cos(\rho_v)) \cdot (3tw) + hw \cdot \rho_{be} \cdot n}{\rho_v}\right) \right. \\ & + \left(tw + \cos(\rho_v) \cdot \left(2tw + \frac{\rho_{be}}{0.731 \cdot tw \cdot fy} \right) \right. \\ & + \left. \left. \left(\cos(\sin(fy)) \cdot \left(2tw + \frac{\rho_{be}}{0.731 \cdot tw \cdot \rho_h} \right) + (2tw) \cdot \rho_{be} \cdot n \right) \right) \right. \\ & + \left. \left. \left(2tw + \frac{\cos\left(\frac{\rho_{be}}{0.731}\right)}{fy \cdot hw} \right) \right) \right) \end{aligned}$$

Equation 25

$$\begin{aligned} \text{delta}A = & \left(\left(\frac{-0.138 \cdot \cos(\cos(hw))}{fy + \sin(fy \cdot hw)} + \left(\frac{-0.138 \cdot n}{fy + \sin(fy \cdot hw)} - \left(\frac{-0.138 \cdot fy}{fy + \sin(fy \cdot hw)} - 0.704 \right) \right) \right) \right. \\ & \left. + \sin(lw) \right) + hw \Big) - tw \end{aligned}$$

Equation 26

$$\begin{aligned} \text{eta}0 = & \cos(\rho_v \cdot 0.051) - (\sin(lw) - \cos(\cos(\sin(lw) - 0.715) \cdot (\cos(\rho_{be}) - \rho_{be})) \\ & \cdot \sin(0.185 + \rho_h) + \sin(-0.098))) \end{aligned}$$

Equation 27

$$\text{delta}eta = \cos(\rho_v \cdot 0.0514) - \sin(lw)$$

$$\begin{aligned} & - \cos \left(\cos \left((tw - \rho_v) \right. \right. \\ & \left. \left. - \frac{tw}{(hw - \rho_{be}) - \cos \left(\frac{(\sin(hw) - \rho_{be}) - \cos(\rho_{be} \cdot -0.774)}{\sin(hw) - 0.774} \right)} \right) \right) \end{aligned}$$

Equation 28

$$\begin{aligned} p = & \cos(-0.103) - \sin((tw - \rho_{be}) - (\rho_h - hw)) - \sin(n) \\ & + \cos((\cos(-0.103(\cos(\cos(-0.103(\rho_v \cdot \rho_h + \rho_{be})))hw) \\ & + \cos(\cos(-0.103)n)) \times -0.103) \times \sin(n)) \end{aligned}$$

Equation 29

$$\begin{aligned} \text{vs}0 = & \sin(tw - tw - fy + \sin((fy - \rho_v) \times \sin(tw)))fy - \cos((fy - fy - \sin((fy \\ & - \rho_v) \times \sin(\sin(\sin((fy - \sin(\sin(tw))) \times \sin(tw))))))tw) \times \sin(\sin(tw))) \end{aligned}$$

Equation 30

$$\psi_0 = fc \cdot \cos(hw)$$

Equation 31

$$\Delta\psi = \sin((n - \rho v) \cdot (0.798 + tw \cdot n) \cdot n)$$

Equation 32

$$\lambda = \sin(lw \cdot \cos(\sin(\rho v) \sin(n - (lw \cdot (lw \cdot \rho v) - lw) - (\rho h - \cos(fc)) \cdot (lw \cdot fc \cdot (tw - hw)))) \cdot \rho v - lw)$$

Equation 33

$$q = \rho v \rho v - (((\rho h - (fy - \rho v \rho v)) - hw) + \cos(\cos(\rho v))) \cdot (\cos(tw) \cdot hw)$$

Equation 34

9. Conclusion

The current thesis develops a multifaceted framework that integrates the Bouc-Wen-Baber-Noori (BWBN) model with data-driven techniques to quantify the hysteretic response of squat RC shear walls in nuclear facilities. In this respect, a dataset of 100 squat RC shear wall specimens was collected from previous relevant experimental programs. This dataset was then used to optimize the BWBN parameters, through the non-dominated sorting genetic algorithm (NSGA-II), in order to accurately predict the hysteretic response of squat RC shear walls. Through exploratory data analysis (EDA), the relationships between the wall geometrical/design characteristics and the BWBN parameters were visualized. The thesis then utilized the BWBN model results through genetic programming to develop equations for the different model parameters.

The results showed that the NSGA-II algorithm through the estimated BWBN parameters was able to adequately predict the hysteretic responses of the experimental squat walls, including their energy dissipation capacities and residual displacements as well as their loading and unloading stiffness values. The EDA results demonstrated also that the BWBN parameters and subsequently the hysteretic response of the walls relied on more than one wall geometrical/design characteristic because, for example, some walls with a similar length showed different strength degradation parameter values. In addition, the BWBN parameters were not significantly related to each other. As such, including all the BWBN parameters to quantify the hysteretic response of the walls was needed for accurate predictions. Moreover, the equations derived using genetic programming had large mean square error values that were deemed not acceptable, and therefore, more experimental results for squat RC shear walls under quasi-static loading are needed to develop equations for the BWBN parameters.

Although the current thesis presented the use of NSGA-II to optimize the BWBN parameters and subsequently quantify the hysteretic response of 100 squat RC shear walls, future experimental studies are still needed to further enlarge the dataset in an effort to enable the use of data-driven techniques to accurately predict such BWBN parameters. Such studies should investigate additional walls with different aspect ratios, material strengths (e.g., high-strength concrete including ultra-high-performance concrete), and axial load levels. Another promising direction for future research could entail the development and validation of numerical models for squat RC shear walls. By using such models, a more comprehensive dataset, representing a wide range of walls, could be generated. The resulting datasets of these studies, including those presented herein, can be also used to develop unique BWBN parameter equations for squat RC shear walls based on their geometrical and design characteristics, thus facilitating their adoption in future editions of relevant design standards.

10. References

1. Abouyoussef, M., and Ezzeldin, M. (2023). Fragility and economic evaluations of high-strength reinforced concrete shear walls in nuclear power plants. *Journal of Structural Engineering*, 149(5), 04023035.
2. Ajavakom, N., Ng, C. H., and Ma, F. (2008). Performance of nonlinear degrading structures: Identification, validation, and prediction. *Computers and Structures*, 86, 652–662.
3. Baber, T. T., and Noori, M. N. (1985). Random vibration of degrading, pinching systems. *Journal of Engineering Mechanics*, 111, 1010–1026.
4. Barbachyn, S.M., R.D. Devine, A. P. Thrall, and Y. C. Kurama. (2020). “Behavior of nuclear RC shear walls designed for similar lateral strengths using normal-strength versus high-strength materials.” *J. Struct. Eng.* 146 (11): 04020252.
5. Betti, M., Facchini, L., and Vignoli, A. (2015, September). Time history analysis of slender masonry towers: a simplified Bouc-Wen approach. XXII Congresso AIMETA, Genova, 111, 257–266.
6. Bouc, R. (1971). Modele mathematique d’hysteresis. *Acustica*, 21, 16–25.
7. Charalampakis, A. E. (2015). The response and dissipated energy of Bouc-Wen hysteretic model revisited. *Archive of Applied Mechanics*, 85(9–10), 1209–1223.
8. Charalampakis, A. E., and Dimou, C. K. (2010). Identification of Bouc-Wen hysteretic systems using particle swarm optimization. *Computers and Structures*, 88(21–22), 1197–1205.
9. Deb, Kalyanmoy. Agrawal, Sameer. Pratap, Amrit. Meyarivan, T. A Fast and Elitist multi-objective Genetic Algorithm: NSGA-II. *IEEE Transactions on Evolutionary Computation (IEEE-TEC)*. Vol. 6. Nr. 2. 2002. Pag. 182–197.

10. Deb, Kalyanmoy. Multi-Objective optimization using evolutionary algorithms. John Wiley and Sons, LTD. Kanpur, India. 2004.
11. Ghobarah, A., and Youssef, M. (1999). Modelling of reinforced concrete structural walls. *Engineering Structures*, 21(10), 912–923. [https://doi.org/10.1016/S0141-0296\(98\)00044-3](https://doi.org/10.1016/S0141-0296(98)00044-3)
12. Gondia, A., Ezzeldin, M., & El-Dakhakhni, W. (2020). Mechanics-Guided Genetic Programming Expression for Shear-Strength Prediction of Squat Reinforced Concrete Walls with Boundary Elements. *Journal of Structural Engineering*, 146(11), 04020223. [https://doi.org/10.1061/\(ASCE\)ST.1943-541X.0002734](https://doi.org/10.1061/(ASCE)ST.1943-541X.0002734)
13. Hidalgo, P. A., Ledezma, C. A., & Jordan, R. M. (2002). Seismic Behavior of Squat Reinforced Concrete Shear Walls. *Earthquake Spectra*, 18(2), 287–308. <https://doi.org/10.1193/1.1490353>
14. Ikhouane, F., and Rodellar, J. (2007). Systems with hysteresis: Analysis, identification and control using the Bouc-Wen model. *Smart structures and materials 2003: Modeling, signal processing, and control*. Hoboken, NJ: John Wiley and Sons.
15. Ikhouane, F., Mañosa, V., and Rodellar, J. (2003). Adaptive backstepping control of a class of hysteretic systems. *Smart structures and materials 2003: Modeling, Signal Processing, and Control*, 5049, 686–695.
16. Ismail, M., Ikhouane, F., and Rodellar, J. (2009). The hysteresis Bouc-Wen model, a survey. *Archives of Computational Methods in Engineering*, 16(2), 161–188.
17. Kottari, A. K., Charalampakis, A. E., and Koumousis, V. K. (2014). A consistent degrading Bouc-Wen model. *Engineering Structures*, 60, 235–240.
18. Kuang, J. S., and Ho, Y.B. (2008). “Seismic behaviour and ductility of squat reinforced concrete shear walls with nonseismic detailing.” *ACI Struct. J.*, 105(2), 225-231

19. Li, B., and Xiang, W. (2011). "Effective stiffness of squat structural walls." *J. Struct Eng.*, 10.1061/(ASCE)ST.1943-541X.0000386, 1470-1479.
20. Manzoori, A., and Toopchi-Nezhad, H. (2017). Application of an extended Bouc-Wen model in seismic response prediction of unbonded fiber reinforced isolators. *Journal of Earthquake Engineering*, 21(1), 87–104.
21. Mao, Y. (2015). *Data visualization in exploratory data analysis: An overview of methods and technologies*.
22. Marano, G. C., and Greco, R. (2006). Damage and ductility demand spectra assessment of hysteretic degrading systems subject to stochastic seismic loads. *Journal of Earthquake Engineering*, 10(05), 615–640.
23. Marano, G. C., Pellicciari, M., Cuoghi, T., Briseghella, B., Lavorato, D., and Tarantino, A. M. (2017). Degrading Bouc-Wen model parameters identification under cyclic load. *International Journal of Geotechnical Earthquake Engineering*, 8(2), 60–81.
24. Masaru, K., and Aiken, I. D. (1997). An analytical hysteresis model for elastomeric seismic isolation bearings. *Earthquake Engineering and Structural Dynamics*, 26(2), 215–231.
25. Oussar, Y., and Dreyfus, G. (2001). How to be a gray box: dynamic semi-physical modeling. *Neural Networks*, 14(9), 1161–1172.
26. Ortiz, G. A., Alvarez, D. A., and Bedoya-Ruíz, D. (2013). Identification of Bouc-Wen type models using multi-objective optimization algorithms. *Computers and Structures*, 114–115(8), 121–132.
27. Pilkoutas, K., and Elnashai, A. S. (1995). "Cyclic behaviour of reinforced concrete cantilever walls, part I: Experimental results." *ACI Struct. J.*, 92(3), 271-281

28. Peng, G. R., Li, W. H., Du, H., Deng, H. X., and Alici, G. (2014). Modelling and identifying the parameters of a magneto-rheological damper with a force-lag phenomenon. *Applied Mathematical Modelling*, 38(15–16), 3763–3773.
29. Pelliciani, M., Marano, G. C., Cuoghi, T., Briseghella, B., Lavorato, D., and Tarantino, A. M. (2018). Parameter identification of degrading and pinched hysteretic systems using a modified Bouc–Wen Model. *Structure and Infrastructure Engineering*, 14(12), 1573–1585. <https://doi.org/10.1080/15732479.2018.1469652>
30. Salonikios, T. N., Kappos, A. J., Tegos, I. A., & Penelis, G. G. (2000). Cyclic load behavior of low-slenderness reinforced concrete walls: failure modes, strength and deformation analysis, and design implications. *ACI Structural Journal*, 97(1), 132-141.
31. Sengupta, P., and Li, B. (2013). Modified Bouc-Wen model for hysteresis behavior of RC beam-column joints with limited transverse reinforcement. *Engineering Structures*, 46, 392–406.
32. Sengupta, and Li, B. (2014). Hysteresis Behavior of Reinforced Concrete Walls. *Journal of Structural Engineering (New York, N.Y.)*, 140(7).
33. Sireteanu, T., Giuclea, M., and Mitu, A. M. (2010). Identification of an extended Bouc-Wen model with application to seismic protection through hysteretic devices. *Computational Mechanics*, 45(5), 431–441.
34. Sireteanu, T., Mitu, A. M., Giuclea, M., and Solomon, O. (2014). A comparative study of the dynamic behavior of Ramberg-Osgood and Bouc-Wen hysteresis models with application to seismic protection of structures. *Computational Mechanics*, 53(3), 451–469.

35. Song, J., Der Kiureghian, A., and Ivanov, L. (2006). A comparative study of the NLSSI and PBEE methods in seismic performance assessment of structures. *Earthquake Engineering and Structural Dynamics*, 35(4), 415–435.
36. Spencer, B. F., Dyke, S. J., Deoskar, H. S., and Sain, M. K. (1997). Benchmark problems in structural control. Part II: active mass driver system. *Earthquake Engineering and Structural Dynamics*, 26(3), 387–395.
37. Wen, Y. K. (1976). Method for random vibration of hysteretic systems. *Journal of the Engineering Mechanics Division*, 102, 249–263.
38. Yusoff, Y., Ngadiman, M. S., & Zain, A. M. (2011). Overview of NSGA-II for optimizing machining process parameters. *Procedia Engineering*, 15, 3978-3983.

Appendix A

